B 3085

LASER INDUCED FORWARD TRANSFER (LIFT) OF METALS, CERAMICS AND COMPOUND SEMICONDUCTORS

Dissertation

Zsolt Tóth

S z e g e d

1991

1. INTRODUCTION 1

1.1. Literature Survey 3

1.2. Aim of the Work 7

2. MODEL CALCULATIONS FOR PULSED LASER HEATING 9

3. LASER INDUCED FORWARD TRANSFER (LIFT) OF METALS 12

3.1. LIFT of Vanadium Films 12

3.1.1. Experimental 12

3.1.2. Results and Discussion 13

3.2. The Role of Film-Support Interface and the Film-to-Substrate Distance 17

3.2.1. Experimental 18

3.2.2. Temperature Calculations 19

3.2.3. LIFT of Poorly Adhering Films 19

3.2.4. LIFT of Well Adhering Films 23

3.3. Conclusions 28

4. LIFT OF Y-BA-CU-O FILMS 30

4.1. Experimental 32

4.2. LIFT of Compound 123 Films by Single Excimer Laser Pulses 34

4.2.1. MgO Support 34

4.2.2. Fused Silica Support 35

4.2.3. Discussion 36

4.3. LIFT of Compound 123 Films by a Scanning Continuous or Chopped Ar^+ Laser Beam 37

4.3.1. MgO Support 37

4.3.2. Fused Silica Support 42

4.3.3. $SrTiO_3$ Support 47

4.3.4. Discussion 48

4.4. Conclusions 50

5. PULSED LASER PROCESSING OF BILAYER THIN FILM STRUCTURES 51

5.1 Experimental 52

5.2. Pulsed Laser Processing of Ge/Se Bilayer Structures.... 53

5.2.1. Glass-Se-Ge Layer Sequence 55

5.2.2. Glass-Ge-Se Layer Sequence 59

5.3. Conclusions 67

6. SUMMARY 69

Appendix 71

References 72

Acknowledgements 75

1. Introduction

In the last decade lasers became common tools in micromachining and production of microelectronic devices. The laser beam is a clean and non-invasive tool able to confine energy into microspace by focusing, and its penetration into the material is precisely tunable. The time scale of the processing ranges from continuous illumination to 10^{-15}s and the power range available is also extremely broad (from mW to TW). For micropatterning various laser induced chemical processes can be applied. The heat due to the laser light absorption (photothermal processing) or alternatively the energy of the photons (photolytic processing) initiates a chemical reaction resulting in the required pattern. Deposition of patterns of dimensions down to the submicrometer range is possible by laser induced chemical vapour deposition (LCVD) or liquid phase deposition while for material removal laser initiated gas or liquid phase etching is the usual technique [1]. These laser-initiated processes are extremely complex: the final result depends on the absorption of the laser light, the kinetics of the chemical reaction, the material transport, in the case of photothermal processing on the temperature distribution formed, etc. For most cases even feedback effects emerge between these parameters leading to self organization processes.

The transfer of thin absorbing films from a transparent support onto another substrate in close proximity by single laser pulses (Laser Induced Forward Transfer =LIFT) offers a straightforward alternative to surface patterning [2-9]. With the LIFT technique (Fig. 1.1), a thin absorbing film of material to be deposited is initially precoated on an optically transparent support. This precoated support

is then placed near to or in contact with another substrate. By irradiating the film with a single laser pulse through the transparent support, the film can be removed from the support (ablation) and deposited onto the selected substrate. The advantages of this technique compared to other available methods are quite obvious. There is no need for complicated and expensive gas handling/vacuum systems and the properties of the surface to be patterned have essentially no influence on the process (which does not mean that - depending on the nature of the actual substrate - the transferred material may not interact further with the substrate). Initial results indicate that LIFT is an inherently clean process since it does not require activation of any chemical reaction: the properties of the prints can be expected to reproduce the quality of the original film even when performed in air [5-9].

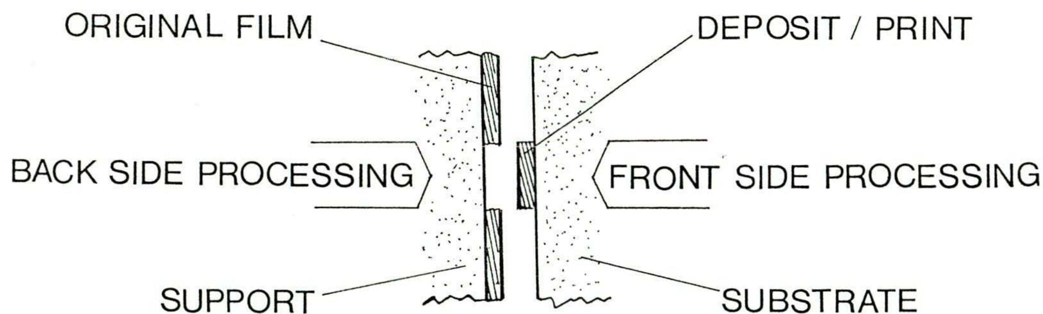

Fig. 1.1. Schematic of LIFT process

Operationally three main elementary steps of the laser induced forward transfer can be distinguished: i) the ablation of the thin films from the support, ii) the transfer/transport of the removed material between the two plates and finally as a last step iii) the deposition of material onto the substrate.

1.1. Literature Survey

The ablation/blow off of thin films from transparent support is a quite old topic with rather extensive literature. The laser machining of thin films [10] has found many applications in the industry. In this overview we shall analyse in details those articles only dealing with ablation as initial step of LIFT. The feasibility of removal of thin metallic and organic films of high resolution by means of a focused laser beam was already demonstrated in the 60-ies [11]. One of the first models of ablation was put forward by Zaleckas and Koo [12]: whenever the evaporation temperature (or alternatively the decomposition or the degasing temperature) of the dielectric substrate is lower than the melting temperature of the film a positive pressure can develop under the film leading to an explosive removal of the metallic film. These authors observed for sufficiently thin metal films ($d<10$ μm) that the machining (ablation) threshold is lower than the damage threshold for the substrate. This model was supported by the experimental results of Andrew et al [13]: the metal removal threshold for Ag, Au, Al, Ni, Cu, Cr from various substrates using XeCl laser pulses was found to be well below the calculated full vaporization fluence level and corresponded more closely to the melting threshold. In contrast to this picture Veiko et al [2, 14] supposed that the removed material formed two phases, namely vapour and liquid. When the thin absorbing film is successively heated to its melting point by laser radiation then it melts and on further heating evaporates intensively, especially after the boiling point is reached. The formed vapour exerts a reactive pressure at the melt/vapour interface which induces a radial melt flow out of the irradiated zone.

The motion of the melt is hindered by surface tension forces, adhesion, viscous friction etc. It is generally accepted in the literature of LIFT [3-7, 15, 16] that in the fluence domain in which the absorbed energy is sufficient to evaporate the layer (at least partially) the mechanism of the film removal is due to thermal ablation combined with propulsion of the film material onto the substrate by the hot vapor formed by evaporating the film at the support-film interface. Bohandy et al. suggested the following sequence of events for the thin metal layer ablation by laser pulses via transparent support [3-5]: (1) The laser pulse heats the front surface of the film (at the support/film interface) until it melts; (2) the melting front propagates through the film and reaches the back surface; (3) at this time or shortly before melting through takes place the front surface becomes superheated or its temperature is close to the boiling point; and (4) at or close to melting through the metal vapor pressure at the front surface propels the molten liquid to the substrate. In situ measurements on the kinetics of the ablation were investigated by Baseman and Froberg [17]. The transmission through thin gold films on optical quartz during laser blow off with 15 ns 532 nm laser pulses was measured. Dramatic changes in transmission indicate the onset of film removal above the ablation threshold. It was experimentally shown for this system that an integrated laser fluence is required to blow off the films which is approximately independent on incident laser fluence, and it is close to that expected to raise the temperature of the film to the boiling point at the film/support interface.

The transport of the material after blow off from the support to the substrate to be patterned has not been investigated experimentally

yet. Time of flight measurements were made only for plasma balls produced by high fluence laser blow off metal films [18]. These plasma balls were used as trace element injection into tokamak accelerators, the removal process ideally resulted in short (100 μsec), intense (10^{10} /cm^3) bursts of neutral metal atoms. Bakos et al found that the plasma ball created in the laser blow off process flew with a velocity of approx.≈$1.75 \cdot 10^4$ m/s which was about five times higher than the thermal velocity of the plasma particles. Very recently a velocity measurement of an excimer laser-ablated aluminum neutral atom plume by dye laser resonance absorption photography was reported by Gilgenbach and Ventzek [19]. Stream velocities measured for neutral aluminum atoms in vacuum ranged from $0.5 \cdot 10^4$ m/s at excimer laser fluences of 1-2 J/cm^2 to $3.4 \cdot 10^4$ m/s at high fluences of 7 J/cm^2. The only theoretical attempt to describe the transport of the material from the support to another substrate was described by Veiko et al [20]: In the case of laser fluences sufficient to vaporize the film the formed vapour current between the two substrates flies in accordance to gas dynamical laws for a nozzle with variable section. As vapour condensation onto the substrate takes place a halo zone is formed. The distribution of condensate in this zone is determined by the condensation intensity and particle sizes. An analytical solution was obtained for the set of equation of gas-dynamics and stream of condensing mono-atomic vapour which described the extension of the halo as a function of the distance d between the two plates. As a rule the halo may be marked from the boundary of the illuminated area $10\text{-}15 \cdot d$ apart. This result show the great influence of the presence of the substrate to be patterned, e.g. if there is 1 μm distance between the support and substrate a spreading of 10-15 μm of the pattern can

be expected.

The role of the process parameters in determining film deposition or pattern formation is largely unknown. In the literature of LIFT [3-7] the deposits are characterized usually qualitatively by optical and electron micrographs. Bohandy et al deposited copper lines of some ten μm width from 0.41 and 1.2 μm source films by 15 ns long $\lambda=193$ nm excimer laser pulses [3]. The four point probe resistivity measurements on copper deposited onto fused silica substrates resulted in values of 3 to 50 times that of the value of bulk copper. Baseman et al investigated in more detail the morphology of the deposited patterns [7]. (Au, Cu, Cr, Ti, Ta, Pt and Ni films were processed with $\lambda=248$ nm, 25 ns long pulses). Generally the morphology changes were systematic. For a given precoated film thickness, at low laser fluences only a small amount of material is transferred. As the laser fluence is gradually increased the transferred material tends to accumulate in relatively thick, isolated structures on top of fine underlying deposits. The reported resolution for this technique was of the order of 10 μm. Baseman et al checked the possibility of obtaining thick deposits through sequential overlapping transfers of thinner films. Neglecting overlay alignment errors the total average deposit thickness was increased linearly with the number of transfers. Fogarassy and coworkers reported a partly successful attempt for transferring Y-Ba-Cu-O and Bi-Sr-Ca-Cu-O superconducting thin films. Superconducting transition was observed in the transferred Bi-Sr-Ca-Cu-O compound only after subsequent thermal treatment in O_2 [6].

In summary, the ideas about laser induced removal/ablation of thin absorbing films described in the literature cannot give a

consistent picture about the process in general. This is due to the fact that only specific conditions and ranges were investigated by several groups. The process of transfer between the support and substrate has not been investigated in situ due to the experimental difficulties. We have only indications that in most cases the deposit formation is a result of the interaction of very high speed supersonic particle stream and the substrate to be patterned. The quality of deposits is not analysed in details in the literature although the applicability of the LIFT technique is greatly dependent on the properties of the patterns deposited.

1.2. Aim of the Work

The primary goals of the present work can be outlined as follows. First to give a critical analysis of the models describing ablation of thin films due to single laser pulses and to compare experimental results and model calculations for various model structures. Second to examine the role of the presence of the adjacent substrate to be patterned for the transfer process. Third to optimize the parameters of the samples and the set-up in order to obtain better quality deposits. Fourth, to explore the benefits and limits of this technique and check the possibility of novel applications.

Accordingly this dissertation is divided into six subsequent chapters. Chapter 2 deals with the basic considerations of temperature calculations for pulsed laser heating of supported mono- or multilayer structures. Chapter 3 is concerned with the LIFT of thermally thin metal layers of strong absorbance, and the bulk of this chapter is devoted the analysis of LIFT, i.e. ablation, transfer and deposition.

The remaining chapters describe some unique applications of the LIFT technique. Chapter 4 deals with the problematics of transferring superconducting thin films of high critical temperatures. In chapter 5 the possibility to deposit compound semiconductors from stacked elemental layers by single laser pulses is demonstrated and some additional aspects of the LIFT technique are shown. Finally in chapter 6 general conclusions are compiled.

2. Model Calculations for Pulsed Laser Heating

It is apparent from the literature that the processes initiated by pulsed laser heating are extremely complex: phase transformations, material transport, and even chemical reactions can compete simultaneously in the nanosecond time-scale. Implicit to these model calculations that no full description of all the events can be given. To follow the events we have calculated the spatial and temporal temperature profiles in mono- and bilayer structure - substrate systems for a whole range of fluences taking into account explicitly all phase changes but neglecting material transport and in the case of bilayers any possible chemical reactions. In spite of these limitations the model calculations give a quantitatively consistent database for the interpretation of the experimental results as shown in the forthcoming sections. Since the onset of the characteristic events (ablation, changes in morphology, synthesis) correlates with the appearance of the new phases, the formation and evolution of these phases is emphasized in the calculations.

Since the lateral dimensions of the processed areas are much larger than the thermal diffusion length (defined by $l=(2D\tau_{ill.})^{1/2}$ where D is the thermal diffusion constant and $\tau_{ill.}$ the processing time) in both the support and the supported films temperature changes are described by the one dimensional heat conduction equation:

$$\frac{\partial T}{\partial t} = \frac{\partial}{\partial z}\left[\frac{\kappa(T)}{\rho(T)c(T)}\frac{\partial T}{\partial z}\right] + \frac{I(z,t)\alpha(T)}{\rho(T)c(T)} \qquad (1)$$

where T, t, κ, ρ, c and α denote the absolute temperature, time, the thermal conductivity, density, specific heat and optical

absorption coefficient, respectively. The last four parameters vary as a function of depth from the upper surface of the layer(s), z across the layer(s)-support system. The spatial and temporal dependence of the intensity is given as

$$I(z,t)=I_0(t)\ (1-R(T))\ \exp[-\alpha(T)z], \tag{2}$$

where $I_0(t)$ is the intensity of the laser beam and R the reflectance of the sample at the wavelength applied. In our case (using Q switched ruby laser) we approximated the temporal intensity with a Gaussian profile:

$$I_0(t)=I_{0,max}\ \exp\left\{-\left[(2\tau-t)/\tau\right]^2\right\} \tag{3}$$

where

$$I_{0,max}=\Phi_{inc}/\tau\cdot(\pi)^{1/2} \quad \text{and} \quad \tau=t_{FWHM}/2(\ln 2)^{1/2}, \tag{4}$$

Φ_{inc} being the incident fluence impinging on the surface of the sample and t_{FWHM} the time of full width at half maximum of the laser pulse.

The solution of Eq. (1) in the general case must be carried out numerically since the physical properties are temperature dependent and phase changes are taking place. Temperature profiles have been calculated using the method of finite differences. This method was adjusted by Jain et al for the calculation of temperature induced by pulsed laser heating of multilayer structures [21]. We have taken into account the temperature dependence of all thermophysical data and incorporated in the model melting and vaporization. The thermal and optical data used are compiled in Table A.1 (p. 71). It should be noted that the material parameters in vapour phase are only coarse

estimates and, thus, the predictions of temperature calculations are realistic until the onset of vapour phase heating.

3. Laser Induced Forward Transfer (LIFT) of Metals

We have systematically studied the response of mm^2-area supported vanadium, chromium and titanium thin films in the low fluence domain for single laser pulses. Incident fluences of 0 - 2.5 J/cm^2 in the case of V and 0 - 1.1 J/cm^2 in the case of Ti and Cr were used; in this fluence range no plasma generation was characteristic. By comparing experimental results with calculated temperature distributions we analyse the role of the support-film interface in governing both ablation and transfer and the dependence of morphology and lateral dimensions of the transferred patterns on the processing fluence and film-to-substrate distance.

3.1. LIFT of Vanadium Films

3.1.1. Experimental

Vanadium films of different thicknesses between 50 and 200 nm were vacuum evaporated onto glass plates which were cleaned by wet chemical methods prior vacuum evaporation. The target substrate to be patterned (a blank glass plate) was placed in contact with the V films. These samples were irradiated both through the support (back side illumination) and through the transparent covering substrate (front side illumination) with spatially homogenized single pulses (λ=694 nm, 20 ns FWHM) from a ruby laser. The shape of the illuminated area was defined by a circular mask of d=3 mm. The energy density impinging on the sample surface Φ_{inc} was tuned in steps of min. 20 mJ/cm^2 using calibrated filters. Due to errors in the measurement of pulse energies and inaccuracies in the determination of the spot dimensions the overall uncertainty in incident fluence values is

estimated to be 10%.

The efficiency of the transfer was characterized with the transmittance of both the deposits (prints) and the ablated areas (remaining films) measured at λ=633 nm. These transmittance data furnish averaged information on the central zone of the patterns (diameter: 0.8 mm). Morphological changes in both the remaining films and the prints were followed in details by mapping the whole processed area by optical microscopy.

3.1.2. Results and Discussion

Optical micrographs of illuminated areas on a vanadium film (A) and corresponding deposits on the covering glass substrate (B) obtained after processing with single pulses of different fluences from the ruby laser are shown in Fig. 3.1. The ablation of the vanadium films started at ~60-80 mJ/cm^2. The value of 60 mJ/cm^2 corresponds to the thinnest film, while the upper value of 80 mJ/cm^2

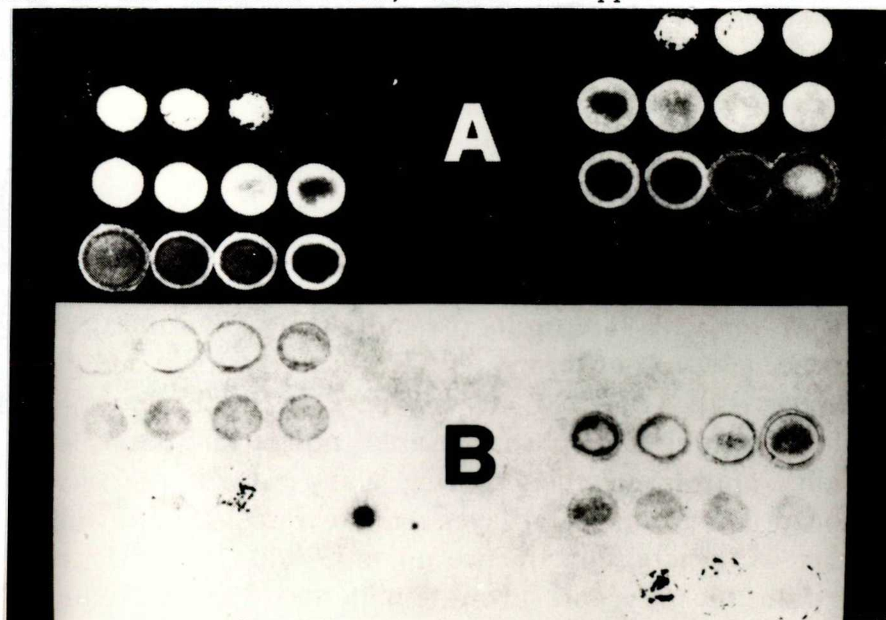

Fig. 3.1. Optical micrographs of ablated areas (A) and corresponding deposits (B). 68 nm V on glass; front side (left) and back side (right) illumination; $30<\Phi_{inc}<2000$ mJ/cm^2

SZEGED

to the thickest film. Processing with fluences above this value up to 300-400 mJ/cm^2 resulted in complete removal of the metal film from the support without any damage of the underlying substrate so we call this fluence range clear ablation window. Both visual and microscope examination suggested that ablation was due to ripping as evidenced by metal chips both on the support and the substrate (see Fig. 3.1). The edges of the ablated patterns were well defined and without traces of melting. The width of the fluence window of clear ablation does not depend significantly on the layer thickness, d, for the applied thicknesses (d≤200 nm), spreading of the ablated area was apparent for thicker films only when processing with increasing fluence.

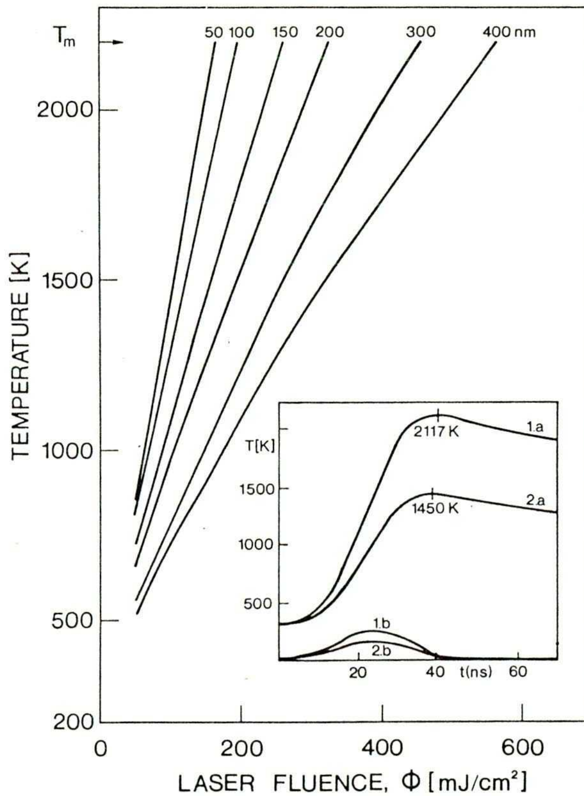

Fig. 3.2. Calculated maximum temperatures in V films of thicknesses ranging from 50 to 400 nm as a function of processing laser fluence. Inset: time evolution of temperature within a V film of 150 nm thickness for Φ = 250 mJ/cm^2 (1.a) and 150 mJ/cm^2 (2.a). (1.b, 2.b) Time scale for the laser pulses

Any comparison between experimental data and model calculations is best done by correlating the sequential events under different fluence levels with the maximum temperatures brought about by the laser pulse. Calculated maximum temperatures in vanadium films of different thicknesses up to the melting point are plotted as a function of the processing laser fluence in Fig. 3.2. In the fluence range of $60 < \Phi_{inc} < 80$ mJ/cm^2 the model calculations yielded maximum temperatures between 970 and 1220 K in the case of the thinnest films (d=50 nm)and between 710 and 850 K in the case of the thickest film (d=200 nm) applied. These values are well below the melting point of vanadium (~2180 K). The good agreement between experimental data and model calculations strongly suggests that in this fluence domain the explosion model put forward by Zaleckas and Koo [12] applies: a positive pressure develops at the support-film interface due to evaporation of layer imperfections and contaminations. Ablation starts when this pressure exceeds a value high enough to separate the film from the support and chip off the film at the edges of the processed area. Since the ablated solid pieces are too cold to stick to the substrate the measured transmittance of the print areas remains in the neighbourhood of 100%. Evidently processing in this clear ablation range results in very effective material removal although no appropriate deposition/printing takes place.

Above the clear ablation window a moisture like thin metal layer remained on the support and got darker with increasing fluence up to ~800-1000 mJ/cm^2. Further increase in fluence results in bleaching and above 2 J/cm^2 the processed surface clears up again indicating an ablation of second type which differs in its mechanism from the previous one. As seen in Fig. 3.1, within the clear ablation window

the diameters of the holes and prints remain equal to the diameter of the processing laser spot on the surface. Increasing fluence results in an increase of the processed area with halo formation and poorly defined prints.

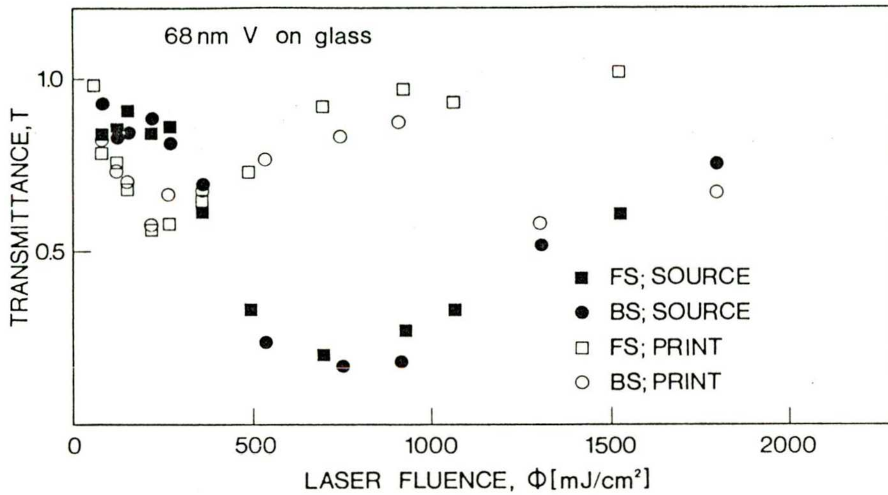

Fig. 3.3. Measured transmittance of ablated areas (source) and deposits (print) as a function of ruby laser fluence for front side (FS) and back side (BS) illumination; 68 nm V on glass

The measured dependence of transmittance, T, of the processed areas of the supported films and the prints as a function of incident fluence reflects the above described sequence more quantitatively. Fig. 3.3 clearly shows that there is no difference between the results of front side and back side processing. These results contradict to the ablation model of moving solid melt boundary put forward by Bohandy and coworkers [3-5]. If this model applied there should be practically no ablation in the case of front side illumination.

3.2. The Role of Film-Support Interface and the Film-to-Substrate Distance

The results of vanadium LIFT gave clear indication that one of the most important parameter in defining ablation and consequently transfer and deposition, too, is the quality of the film-support interface. The interface can be characterized by the cleanness/amount of contaminations which practically determines the adherence of the film to the substrate. Keeping in mind that our examinations on V LIFT justified the model of explosion the cleanness of the interface should determine the ablation in two ways: the amount of contaminations defines the amount of vapour able to form at the interface and on the other hand it defines the force which is needed to tear off the film from the support. There are two trivial ways to modify the interface: 1) cleaning different ways the support before evaporating the thin film and 2) selecting different support/film materials. For a comparative study better suits the first possibility: if different material supports/films are chosen not only the interface but all optical and thermophysical properties are modified, too. We have investigated both possibilities: the same support-film pair was used but the support was cleaned in different way before evaporation. In another series of experiments the same support with different metal layers was also studied.

As pointed out in the introduction no experimental investigation has been made in order to study the process of the transfer itself. The difficulties of in situ measurements are obvious: a fast non-invasive recording of movement of vapour and particles in the chink between the support and the substrate is required. One

possibility for velocity measurements could be the technique of Laser Doppler Anemometry (LDA) [24] since velocity measurement of moving particles is possible in a very broad range by this simple optical way in a microspace. One of the main parameter of the material transport the role of which can be investigated experimentally relatively easily is the transfer length, i.e. the film-to-substrate distance. In the experiments described in the literature the supported films were held in contact with [3-6] or "near to" [3, 7] the substrate. In the following part we present our experimental results and discussion on concerning the role of film-support interface and the film-to-substrate distance.

3.2.1 Experimental

The optical set-up for the present experiments was the same as applied for V films. Two sets of titanium films of the same thickness (200 nm) but of different adhesion to the glass substrates and standard optical chrome masks (HOYA) of 173 nm thickness with very good adhering properties served as source materials. Prior to vacuum evaporation for the first set of Ti films the glass was cleaned solely by wet chemical methods only while for the second set of Ti an additional cleaning step in glow discharge was applied. The film-to-substrate adherence was controlled by the Scotch tape test. After wet chemical cleaning the films could easily be removed indicating poor adherence while glow discharge cleaning always yielded well adhering films. The substrate to be patterned (a glass plate) was placed in a controlled distance from the Ti and Cr thin films. The film-to-substrate distance was adjusted interferometrically in steps of approximately 5 μm using a low power He-Ne laser beam impinging on

the front side of the film across the transparent substrate with the angle of 20°. This setup allowed only back side processing of the sample i.e. the irradiation through the glass support by the ruby laser light. The shape of the illuminated area was defined by a mask of $1.8x1.8\ mm^2$ square.

The ablated areas and the deposited patterns similarly to the V samples were characterized by measured transmissions and optical microscopy.

3.2.2. Temperature Calculations

The calculated maximal temperature curves are given as a function of incident fluence in Figs. 3.4 and 3.5 referring to both supported and free standing Ti and Cr films. The reason for this is that, strictly speaking, the supported film model can only be applied until no material removal occurs, i.e. below the ablation threshold. Above the onset of material transport the actual temperature lies between two limiting values: it is probably significantly higher than that calculated from the supported film model but is lower than that predicted by the free standing film model. During transfer the actual temperature of the removed material may considerably differ from that of the remaining layer depending on the time delay between the start of the laser pulse and the onset of ablation. Since with increasing fluence this time delay decreases [17] the (local) temperatures approach the upper limit under high fluence conditions.

3.2.3 LIFT of Poorly Adhering Films

The ablation of the poorly adhering titanium films started at $\sim 100\ mJ/cm^2$ as indicated in the upper part of Fig. 3.6 by the abrupt

change in measured transmittance of the ablated areas. Similarly to the results obtained for V films clear ablation was observed in the 100-240 mJ/cm^2 window. Due to chips remaining on the support intermediate transmittance values between 0.0 and 1.0 were occasionally observed (Fig. 3.6 upper part 100 < Φ < 200 mJ/cm^2). The edges of the ablated patterns were well defined and without any trace of melting. In the fluence range of 100 < Φ < 240 mJ/cm^2 the model calculations, assuming supported films, yielded maximum temperatures between 1140 and 1941 K, i.e. the ablation similarly to V films started below the melting point of titanium (1941 K). Naturally this means that the reason of clear ablation of poorly adhering titanium is the same as discussed above for vanadium.

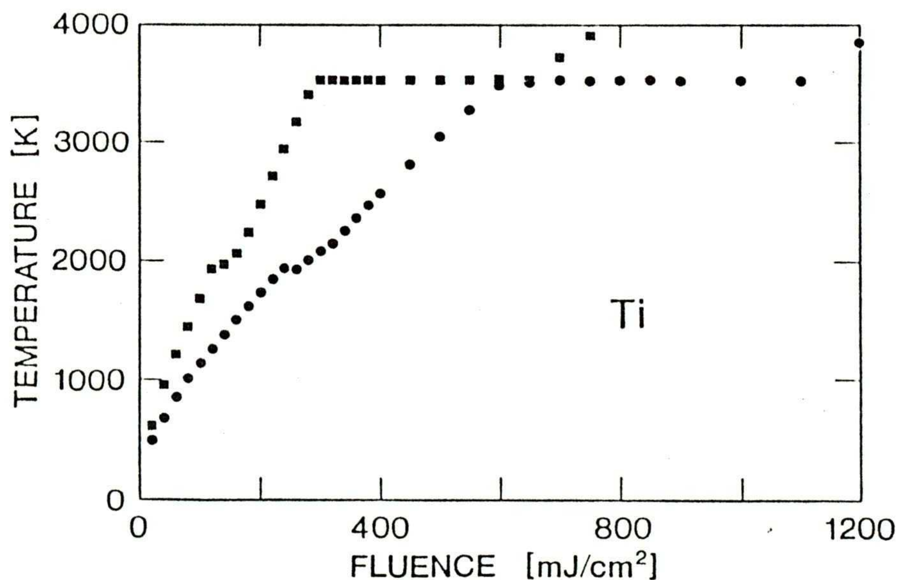

Fig. 3.4. Calculated maximum temperature vs. incident fluence for 200 nm thick supported (●) and free standing (■) titanium films

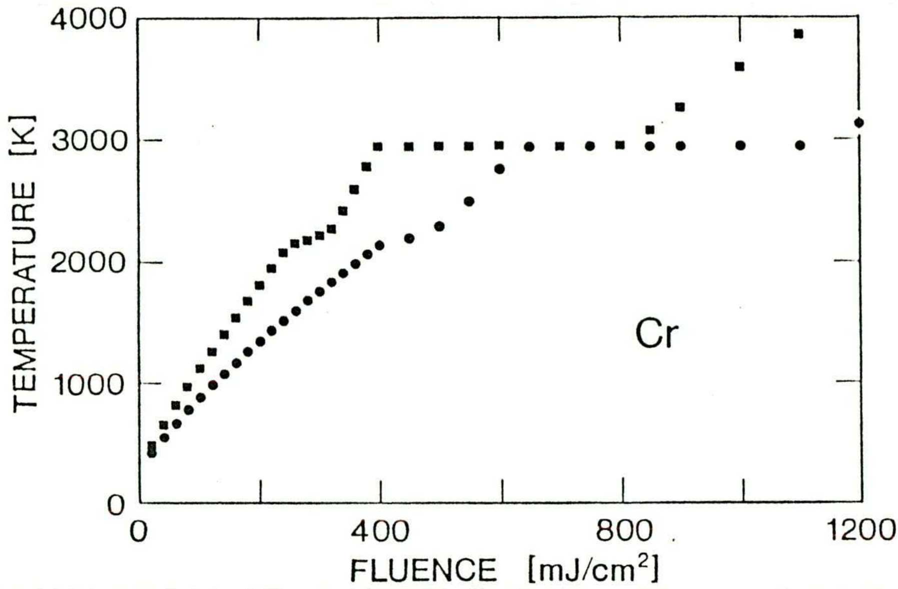

Fig. 3.5. Calculated maximum temperature vs. incident fluence for 173 nm thick supported (●) and free standing (■) chromium films

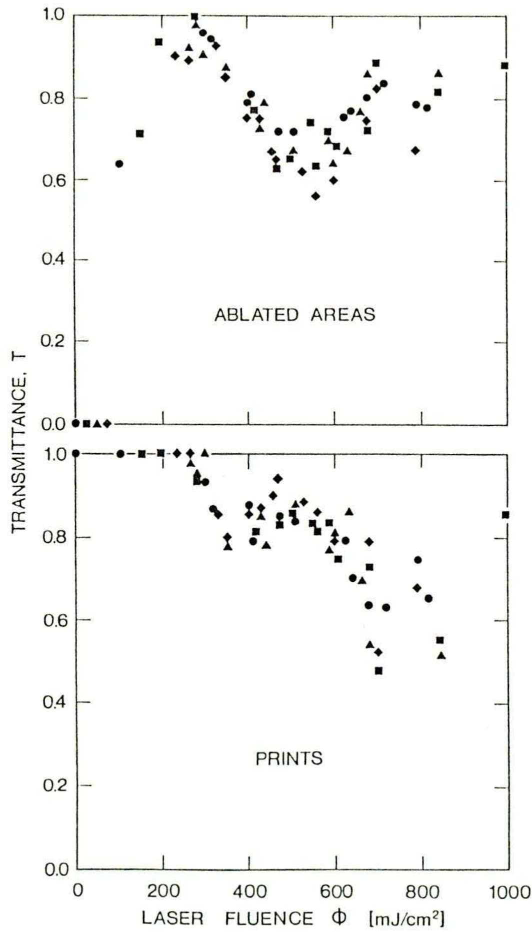

Fig. 3.6. Measured transmittance of the ablated areas and the corresponding prints of poorly adhering Ti films as a function of incident laser fluence. Spacing: 15 (◆), 35 (▲), 45 (■) and 55 (●) μm

Above 240 mJ/cm^2 the transmittance of the print areas started to decrease indicating the onset of deposition; the prints consisted of resolidified splashes. The contours of the prints were poorly defined and the material spread beyond the illuminated area. With increasing fluences up to ~ 550 mJ/cm^2 the ablated areas got darker due to the formation of a hazy layer on the support. As shown in Fig. 3.4 the temperature calculations for supported Ti films indicated the onset and completion of the melting at 240 and 260 mJ/cm^2, respectively. Therefore, the darkening of both the prints and ablated areas can be explained by the onset of film melting. There are several consequences of melting in this fluence range. The efficiency of ablation significantly decreases since the continuous film material forms droplets upon melting and the propelling gas escapes via the interdroplet space. As a consequence the blow off becomes discontinuous and can not transfer larger pieces. On increasing the fluence the time period necessary for complete melting [17] and the viscosity of the molten material decreases resulting in accelerated droplet formation and less effective ablation. Consequently an increasing amount of film material remains on the support as evidenced by the decreasing transmittance of the ablated areas. Since the particles removed are in the molten state they are inherently more adhesive and remain on the substrate. Therefore whenever melting is the characteristic event the effectivity of material removal is decreased and still print formation commences.

A further increase in laser fluence above 550 mJ/cm^2 resulted in bleaching of the processed area and concomitant darkening of the prints. Material spreading beyond the illuminated area, first observed at 200 mJ/cm^2 processing, became more extensive in this fluence range

leading to considerable extension of the ablated area compared to that observed for low fluence processing. The onset of the boiling is clearly indicated by the temperature calculations, even the lower limit (supported film model) shows the beginning of boiling at 600 mJ/cm^2. While melting hampers the ablation the formation of vapour phase increases the efficiency of both the removal and the transfer. Due to the fast heating melting and evaporation takes place in the nanosecond time scale and the transfer develops in a rather turbulent manner in this fluence domain; the extreme speed and associated shock waves push the material far beyond the illuminated area.

Note that in the case of poorly adhering films the transfer yield characterized by the measured transmittance of both prints and ablated areas (cf. Fig. 3.6) proved to be independent of film-to-substrate distance within the accuracy of the measurements in the applied fluence range.

3.2.4. LIFT of Well Adhering Films

The processing of well adhering Ti films and chrome masks resulted in essentially the same trends with differences in threshold fluences only. In the followings these trends will be demonstrated for standard optical chrome masks.

When processing optical chrome masks with single laser pulses of fluences below 250 mJ/cm^2 no detectable changes were observed. As shown in Fig. 3.7 ablation started above this value and was followed by an approximately linear increase in the transmittance of the ablated areas between 350 and 600 mJ/cm^2. The ablated patterns preserved the outline of the processing beam with constant transmittance in the centre and less well defined borderlines

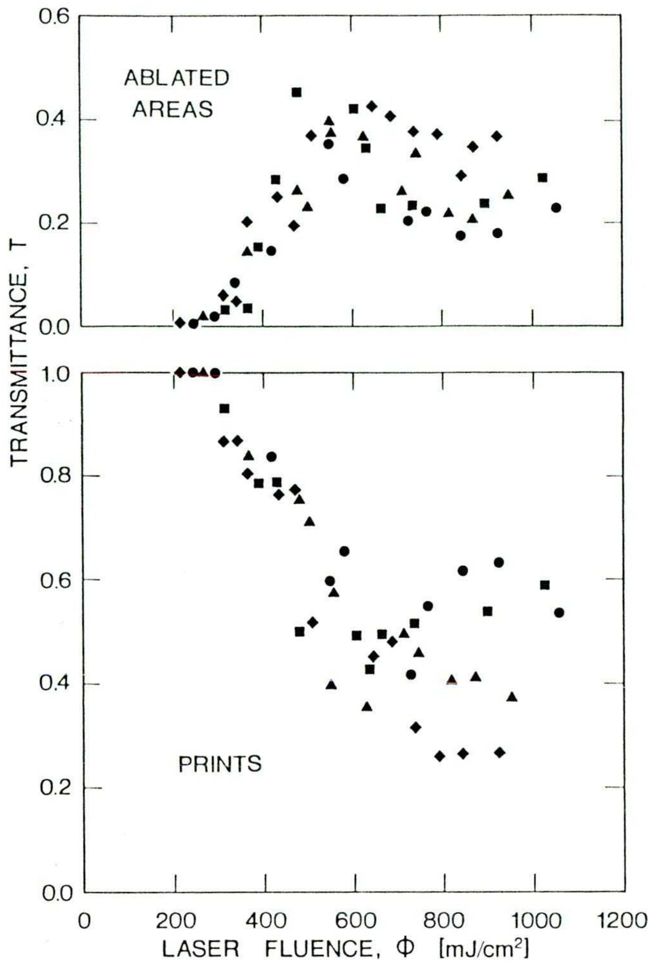

Fig. 3.7. Measured transmittance of the ablated areas and the corresponding prints for the chrome mask as a function of incident laser fluence. Spacing: 15 (◆), 35 (▲), 45 (■) and 55 (●) μm

spreading over 0.1-0.3 mm. Optical microscope examination revealed that unlike in the case of poorly adhering films the ablation was incomplete in this fluence domain over the entire processed area; the film was removed and transferred locally in form of isolated holes and islands, respectively. With increasing fluence the removed portions of the irradiated film became larger and more numerous until maximum transmittance was obtained. This sequence of events as a function of laser fluence is exactly the same as that of reported by Baseman and coworkers for 370 nm thick gold (Figs. 1 in [15] and [16]) and 200 nm thick chromium films (Fig. 3 in [15]). Material deposition commenced

at approx. 300 mJ/cm^2. With increasing fluence between 300 and 600 mJ/cm^2 the transmittance of the prints gradually decreased.

A comparison between experimental results and temperature calculations suggests that in this low fluence domain the mechanism of both ablation and transfer can be interpreted in terms of the explosion model, too [12]. An obvious difference between poorly and well adhering films is that ablation starts at tiny seeds in this latter case. Just above the ablation threshold the fraction of the ablated areas is rather small (the transmission is negligible). With increasing fluence the effectivity of the removal gradually increases since the pressure of the encapsulated vapour bubbles increases with increasing temperature and weaker forces are needed to sheer the layer against cohesion. This results in monotonously increasing transmittance of the ablated areas. The local temperature of the floating areas above the vapour bubbles can be significantly higher than the macroscopic average value. Consequently the ablated fragments may be hot enough to stick to the substrate leading to rather efficient transfer yields. This mechanism is operative until local melting extends to the whole area.

In the range of 550-800 mJ/cm^2 the transmittance of the ablated area decreased with increasing fluence (darkening) while above this range further bleaching was observed. These trends are similar to that of measured for poorly adhering films and can be explained similarly. The results of the temperature calculations indicate that in the case of the supported film melting starts and completes at 400 and 480 mJ/cm^2, respectively, and the boiling point is reached at 660 mJ/cm^2. These figures strongly suggest that darkening correlates with the onset of melting, while the beginning of bleaching at higher fluences

with the onset of evaporation. It should be noted that a similar darkening and subsequent bleaching of the ablated area of thin chromium films has also been observed although not commented by Baseman and coworkers [15].

Unlike in the case of poorly adhering films a clear dependence of the transmittance of both prints and ablated areas was observed on film-to-substrate distance above approx. 550 mJ/cm^2. The highest transmittance values for the ablated areas were measured with the narrowest spacing ($d<15$ μm). With increasing distance the transmittance decreased to a minimum value of $T \simeq 0.17$ ($d=55$ μm, upper part of Fig. 3.7). This value was less than half of that observed in the case of direct contact. Complementary trends were observed for the prints: with increasing distance their transmittance increased. For a distance of $d=15$ μm the transmittance monotonously decreased throughout the whole fluence range to a value of $T \simeq 0.26$. In the case of $d = 35$ μm a plateau was observed in the range of 600-1000 mJ/cm^2 with $T = 0.4$, whereas the transmittance gradually increased in the same fluence range for larger spacings, the increase being more pronounced for $d = 55$ μm.

The transmittances of ablated areas and prints are compared for low (350-400 mJ/cm^2: closed symbols) and high fluences (850-960 mJ/cm^2: open symbols) as a function of film-to-substrate distance in Fig. 3.8. Unlike for the low fluences which brought about no significant change, there was a steep increase and decrease in the respective transmittances of prints and ablated areas in the high fluence range.

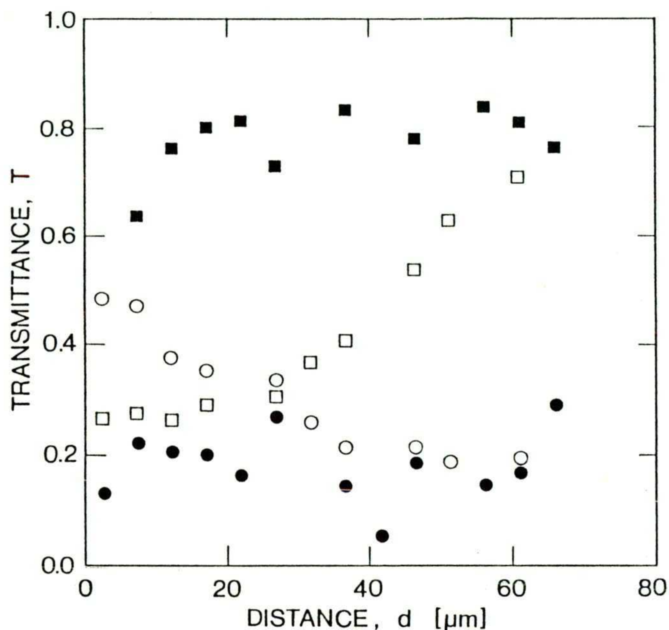

Fig. 3.8. Measured transmittance of the ablated areas (o, ●) and the corresponding prints (□, ■) for the chrome mask as a function of film-to-substrate distance, d for Φ = 350-400 mJ/cm^2 (closed symbols) and 850-960 mJ/cm^2 (open symbols)

As determined by optical microscopy processing at narrow spacing (d ≤ 15 µm) resulted in prints without any macrostructure for all fluence levels, while at larger spacings a structured pattern was formed. This latter pattern had a central zone of uniformly distributed small islands and radial arms formed by elongated islands of the printed material. The print pattern was framed by a circular halo spread further out, e.g. its outer diameter increased from 3 to 4 mm on increasing the spacing from 15 to 65 µm and using a fluence of 740 mJ/cm^2. At fluences of approx. 1 J/cm^2 the central zone of the print patterns became bleached when processed in distances over 25-30 µm. In the case of spacings over 60-70 µm the template area became

nearly transparent surrounded by a dark zone near to the halo frame.

Similar structural changes were observed in the ablated area, but above 600 mJ/cm^2 the appearance of the radial structure started at narrower spacings than in the prints. Near to 1 J/cm^2 the grey illuminated area was surrounded by dark edges and 6-7.5 mm apart from the centre the displaced material formed a deposition frame on the metal surface corresponding to the halo ring on the print face.

3.3. Conclusions

In the case of films with poor mechanical and thermal contact to the support an abrupt ablation threshold is observed. At fluences just above this threshold the whole irradiated area is removed in form of solid pieces resulting in complete ablation without printing. The lack of print formation is consistent with the notion that the removed pieces are too cold to stick onto the substrate. When reaching the fluence level which brings about melting the effectivity of material removal decreases while print formation commences. Processing above the fluence value enough for formation of vapour phase increases the efficiency of both removal and transfer.

The ablation of well adhering films starts at tiny seeds; with increasing fluence the effectivity of both removal and transfer monotonously increases until local melting extends to the whole area. Similarly to the poorly adhering films darkening of the remaining layer correlates with the onset of melting and the start of bleaching at higher fluences with the onset of subsequent evaporation.

Poorly and well adhering films show different dependence on the film-to-substrate distance. In the former case the transfer yield

proved to be independent between 0 and 60 μm throughout the fluence range studied while in the latter case a clear dependence of the transmittance of both prints and ablated areas is observed as evaporation becomes dominant. With increasing distance the transmittance of the ablated areas of well adhering films decreases and that of the prints increases. The most effective transfer preserving the source pattern is produced processing well adhering source films held in contact with the substrate to be patterned with fluences corresponding to temperatures near to the boiling point.

4. LIFT of Y-Ba-Cu-O Films

The new ceramic rare earth - alkaline earth - copper oxide, high critical temperature (T_c) superconductors have generated a great upsurge of research activity since their discovery [25]. The preparation of bulk superconducting materials by mixing of elements as oxides or as easily decomposing compounds is well understood. However the mechanical, chemical and electrical properties of bulk ceramic superconductors do not allow widespread applications. The potential applications involving superconducting thin films, such as hybrid superconducting/semiconducting circuits and microwave/millimeter wave devices seem to be more imminent than the applications of bulk materials. Nowadays numerous techniques are developed to prepare superconducting thin films [26]: the most frequently used beeing sputtering, electron beam evaporation, laser ablation; other methods of limited usage are spray pyrolysis of organometallic compounds, molecular beam epitaxy (MBE), and chemical vapour deposition (CVD). The patterning of these prepared films is rather problematic since these types of materials are chemically unstable (e.g. they react with water) and, thus a number of conventional lithographic methods combined with etching cannot be applied. The LIFT technique could be an alternative for depositing patterns from sources as precoated ceramic films onto different surfaces. As mentioned in section 1 Fogarassy et al. demonstrated the possibility of transferring Bi-Sr-Ca-Cu-O thin films by the LIFT technique; in these experiments superconducting transition could only be observed in the transferred Bi-Sr-Ca-Cu-O compound after subsequent thermal treatment in O_2 [6].

The primary concern in the transfer/deposition of Y_1-Ba_2-Cu_3-$O_{7-\delta}$ thin films is the control of the correct metallic stoichiometry (Y:Ba:Cu=1:2:3) and the uniform thickness of deposits. In addition, superconductivity can only be achieved when the crystal structure and amount of oxygen in compound 123 is carefully controlled. Compound 123 has two crystal structures namely orthorhombic and tetragonal, which differ from each other in their oxygen content: tetragonal has <6.5 moles and orthorhombic 6.5-7 moles of oxygen, respectively. The orthorhombic phase is superconducting while the tetragonal is not. These requirements mean that the deposition conditions, source films, supports and substrates need a careful study since all these parameters affect the film composition and/or structure.

In this chapter we report results on a systematic series of laser induced forward transfer of $Y_1Ba_2Cu_3O_{7-\delta}$ high T_c superconducting films. In order to produce superconducting patterns the LIFT technique should be optimized; in this particular case one has to develop a process suitable for producing well defined patterns with strictly determined stoichiometry and structure. The low thermal conductivity [27, 28] and the relatively high optical absorption in the UV and visible [6] of the superconducting ceramics allows the use of longer pulse durations or even cw laser processing to reach the required heating rate for LIFT conditions. So, in addition to pulsed laser patterning, a study of direct writing by cw lasers seems to be of great promise.

The key parameter in determining superconducting properties is the thermal history of the pattern. Since the components of the superconducting ceramics have rather different mobility at high temperatures (T>~1000 K) the resulting stoichiometry will greatly

depend on the heating rate during transfer. This frozen-in structure depends on, among other parameters, the cooling rate after reaching the substrate. Therefore, the first step should be assessed extremely carefully when modelling the temperature evolution for a real set of parameters. The laser parameters and the thermal and optical characteristics of the support (quartz, MgO, $SrTiO_3$), the superconducting layer and the substrate play a decisive role in governing the ablation process and in defining the properties of the obtained patterns.

As a first approximation of the experimental realization of LIFT of superconducting patterns, stripes should be produced which preserve the stoichiometry of the target films, and the superconducting structure can be obtained by post annealing. Needless to say the ultimate goal is the single step direct writing of superconducting stripes in situ. When succesfully realized this technique commands interest in a broad field of applications, e.g. producing Josephson junctions, squids etc.

4.1. Experimental

Polished single crystal MgO, $SrTiO_3$ sheets and fused silica were used as support materials. Onto MgO and $SrTiO_3$ supports the superconducting 123 films of 86-91 K critical temperatures were deposited by laser ablation. The thicknesses of these films in our experiments varied between 0.2 and 1.1 μm. Stoichiometric but non-superconducting films of thicknesses ~ 0.3 and ~ 1μm were deposited onto the fused silica surfaces by spray pyrolysis and by laser ablation. Finally the films were covered with Si wafer plates or

polished MgO sheets which served as substrates to be patterned.

In the first series of experiments the samples were irradiated with single laser pulses of a XeCl excimer laser (λ=308 nm, 10 ns FWHM, ~120 mJ pulse energies) through a diaphragm and a cylindrical lens so that the laser affected areas formed lines of 0.2-0.5 mm. The films were always illuminated across the original support (back side illumination). The incident energy on the sample surface was adjusted by filters and monitored by a calibrated photodiode after each pulse. Since the spatial beam profile on the sample surface was not homogeneous only the average fluence could be calculated ranging up to 2.5 J/cm^2.

In the second series of experiments a TEM_{00} beam of a cw Ar^+ laser (λ=514 nm) was focused onto the support-film interface (back side illumination) and scanned with velocities from 100 μm/s to 3 mm/s. Experiments were done using continuous or chopped illumination, in the latter case the pulse duration could be set by an electrooptical modulator. The shortest available pulse length was 1 μs, and the highest repetition rate of the pulses was 500 Hz. The focal radii defined by the 1/e^2 decrease in intensity were 1.5, 3 and 5 μm, the applied powers were between 50 mW and 1 W.

The ablated areas and the transferred patterns were characterized by optical and scanning electron microscopy and a semiquantitative elemental analysis was made by electron microprobe (EDAX). In the case of contiguous deposits the resistivity was measured in the 10-300 K regime with the four point method.

4.2. LIFT of Compound 123 Films by Single Excimer Laser Pulses

4.2.1. MgO Support

When processing compound 123 films deposited by laser ablation onto MgO with thickness of 200 nm the events were rather similar to those observed when processing of well adhering films. This is not surprising since these films were grown epitaxially onto the support surface and so the adherence of these films were rather good. The ablation started in localized seeds at ~350 mJ/cm^2. The number of seeds and their sizes increased with increasing fluence leading to more efficient material removal. According to this trend more and more material could be deposited onto the substrate surface but no continuous layer was formed. The prints consisted of separate molten fragments in a wide fluence range. Continuous deposit formation on the substrate required high fluence processing of 2.5-3 J/cm^2 incident fluence but this deposit was usually rather thin, most of the material being spread beyond the illuminated area and stick to the original support and the substrate in form of droplets.

When processing compound 123 layer of 1.1 μm thickness on MgO support no deformation of the original film could be observed up to a fluence processing level of 1.5 J/cm^2. At fluence about 1.5 J/cm^2 the film separated from the support but did not break/ tear off. Even higher fluences up to 3 J/cm^{2}were not sufficient to initiate material removal. This behaviour can be explained easily with the sample geometry and the material properties: compound 123 is a relatively good thermal insulator (2.5-3W/mK [27, 28]) and absorbs nearly the whole amount of light of the excimer laser on the light affected surface ($\alpha \simeq 3 \cdot 10^7$ 1/m [6]); therefore, the pulsed laser illumination

leads to great temperature gradient formation. On the other hand, the MgO support is at least an order of magnitude better thermal conductor than the 123 ceramics. Consequently the bulk of the heat generated at the MgO-123 interface is conducted towards the MgO support and not into the layer, and so the heating of the layer by the laser pulse cannot be as effective as in the case of metal films. Having a film of 1.1 μm thickness only a small part of the film can be evaporated close to the support-film interface even in the case of high fluence illuminations. Since this film is relatively thick the generated vapour is trapped between the support and the film and cannot set up a pressure sufficient for breaking the film; however a clear separation between the compound 123 layer and the support is observed.

4.2.2. Fused Silica Support

Using fused silica supports of low thermal conductivity (1.1 W/mK) instead of MgO the effectivity of laser heating of the layer increases. This corresponds very well to the experimental results; the first ablation threshold is 200 and 340 mJ/cm^2 for the 300 nm thick and the 1 μm thick layers, respectively, produced by spray pyrolysis. Since compound 123 films do not adhere well to the surface of quartz the behaviour of these structures strongly correlates with the nature of poorly adhering metal thin films. Indeed, total ablation of the layer in solid phase takes place above fluences of 500 and 630 mJ/cm^2, but melting/deposition starts only above 1100 and 2100 mJ/cm^2 processing for 300 and 1100 nm thick compound 123 layers, respectively. In this case the window of clear ablation is very broad as a consequence of the great temperature gradient arising in the compound 123 layer due to its strong absorbance and poor thermal

conductivity. Since the upper part of the layer which faces the target substrate to be patterned is cooler, sticky deposits can be obtained with complete melting of the whole layer. Obviously higher energy density is needed for melting to occur in this inhomogeneously heated layer than in the case of homogeneous heating. The fluence difference between homogeneous and inhomogeneous heating is used to raise the temperature above the melting point in the hotter parts of the layer so long melting takes place in the cooler parts. The deposits/prints can be characterised similarly as processing of films on a MgO support. The deposits consist of separated islands of 2-10 μm size and only high fluence which is enough to vapourize the film results in more or less continuous thin layer formation.

4.2.3. Discussion

The main problem in the application of excimer laser induced forward transfer of compound 123 films is that the formation of well adhering deposits and a contiguous layer structure in a single step is not possible. As demonstrated above ablation and transfer of continuous solid pieces is only possible from fused silica support, but these fragments do not stick to the substrate; when print formation occurs the greater part of the deposits forms isolated droplets. To reach more homogeneous deposition more homogeneous and slower heating is required which has put forward the idea of using a scanning focused continuous wave laser heating.

4.3. LIFT of Compound 123 Films by a Scanning Continuous or Chopped Ar^+ Laser Beam

4.3.1. MgO Support

When using continuous illumination no difference was found in the obtained patterns using different scanning speeds in the applied regime. This is not surprising since the thermal diffusion length for the smallest dwell time (defined as beam diameter/scanning velocity) is at least an order of magnitude greater than the beam size. This means that the timescale of the thermally activated events taking place in cw LIFT is much less than the dwell time. A steady state geometry and temperature distribution can be defined providing we fix the coordinate system to the moving beam; in this case the cw laser light beam heats up the layer gradually and the supposed mechanism is thermal evaporation of the film and recondensation onto the colder parts of the substrate.

Having 200 nm and 1μm thick compound 123 layers laser-sputtered onto MgO support the threshold of film modification was detected at 150 and 120 mW, respectively, illuminating the films at a focal size of the Ar^+ beam $2w_0$= 3 μm. The lower threshold for thicker films can be understood by the fact that the thicker layer absorbs the entire power with no significant losses by reflection, while the thinner layer is slightly transparent at this wavelength, the light penetration depth being ($1/\alpha \sim 170$ nm at λ=514 nm [6]) comparable to the thickness of the thinner film, and so the absorbed power is significantly less in this case.

Deposition commenced at 320 and 150 mW and continuous stripes of good morphology and well defined edges were produced in the 450-800 and 200-350 mW domain in the case of 200 nm and the 1 μm films,

respectively. In Fig. 4.1 a SEM micrograph of two stripes deposited onto MgO surface is shown. The processed area was never completely clean, a hazy thin layer remained on the processed areas in each case.

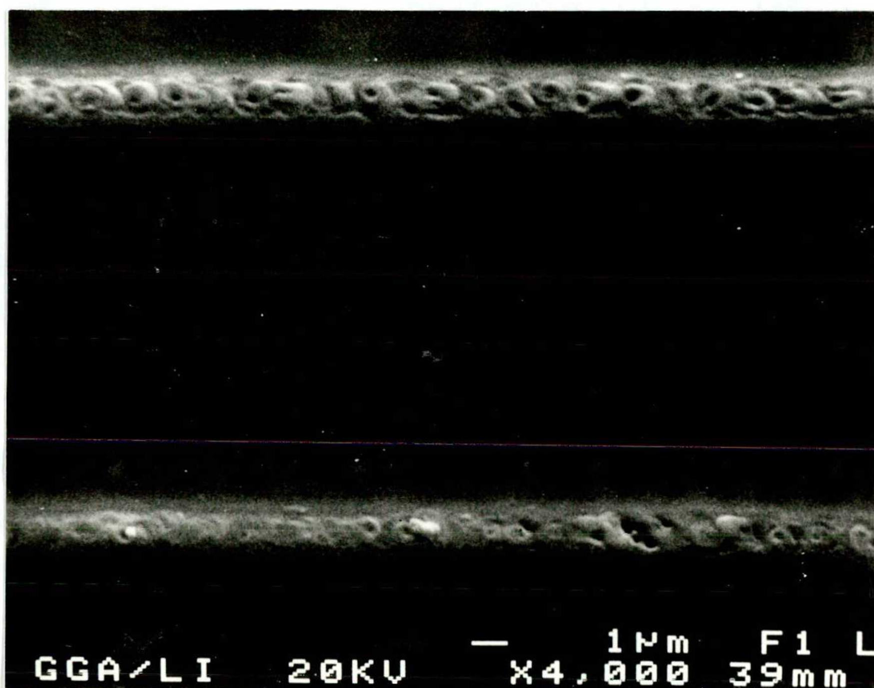

Fig. 4.1. Lines deposited by scanning cw laser beam, $2w_0$=3μm, v_{scan}=3 mm/s. The incident power was 474 mW (lower trace) and 538 mW (upper trace)

The cw LIFT from MgO support did not preserve the stoichiometry of the initial film. As EDAX examinations revealed there was a deficiency in Ba content and the Y component was completely missing from the deposits.

Above 800 mW for 200 nm thick and 350 mW for 1 μm thick compound 123 films the processing also affected the MgO support. As shown in Fig. 4.2 large drops of MgO were deposited on the top of the compound 123 line. This event is a clear indication of the extremely high temperature, since such drops can only be formed by the melting of MgO (melting point of MgO is 3125 K [22]). On the other hand, the preferable process for the MgO droplet formation is recondensation

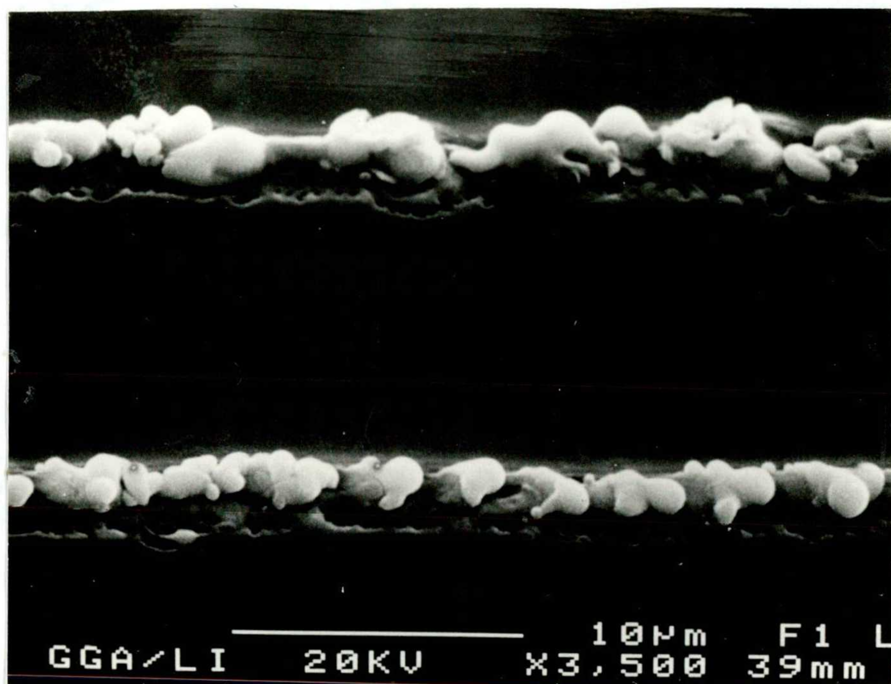

Fig. 4.2. Lines deposited by scanning cw laser beam, $2w_0$=3μm, v_{scan}=3 mm/s. The incident power was 930 mW (lower trace) and 1076 mW (upper trace)

from saturated vapour indicating that the temperature must be close to the boiling point of MgO (~3870 K [22]).

Faster heating rates can be achieved locally when illuminating the film with pulse series in such a way that the neighbouring pulses process overlapping areas. The degree of overlapping is defined by the scanning velocity ($v_{scan.}$), the repetition rate of pulses (f) and the size of laser beam (w_0), whenever the length of a single pulse is much shorter than the dwell time. Let us define a quantity which describes the degree of overlap (O) as follows

$$O = \frac{2\, w_0 \cdot f}{v_{scan.}} .$$

The value of O gives the number how many times the laser pulses reached the central part of the line. Obviously to reach overlapping areas the value of O should be larger than 1. The larger the parameter

O, the more continuous deposition can be achieved; however, on the other hand, smaller O values are required to obtain quicker heating of the still unprocessed areas. In the experiments described below the parameter O was varied between 1 and 10. In this regime no significant alterations were found between the stoichiometries of the deposited lines. For all results presented below for MgO support the scanning velocity, the beam diameter and the repetition rate were 235 μm/s, 6 μm and 200 Hz, respectively, so the factor of overlapping, O was the value of 5.1.

To obtain stripes of good morphology two parameters were found to have an important role: the processing intensity and the duration of the pulses. In Fig. 4.3 the regime for continuous deposition of good quality stripes is presented. When processing with low powers and

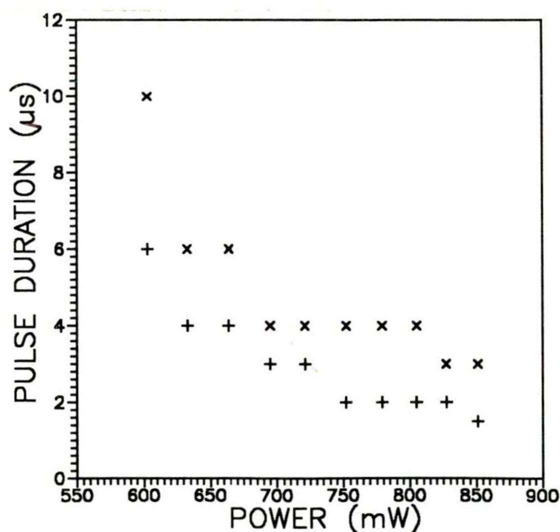

Fig. 4.3. Thresholds of the onset of continuous stripe formation (+) and damage/evaporation of the support material (MgO) (x). The area between + and x symbols represents the regime for deposition stripes of good morphology.

small pulse durations (below the + symbols) the deposits contain small separated drops. The area between the + and x symbols represents the regime of continuous line formation. Above this domain the stripes

become broken and MgO removal and deposition occurs. This trend is illustrated in Fig. 4.4 which shows 5 stripes made with the same power 779 mW, but different pulse durations.

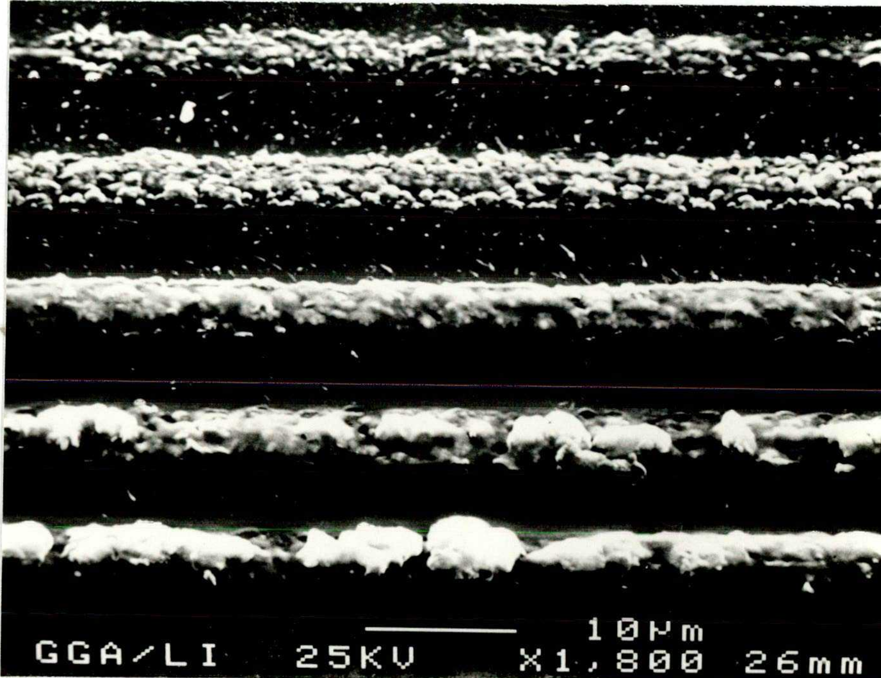

Fig. 4.4. Lines deposited by Ar^+ laser pulse series. $2w_0$=6µm. The incident power was 779 mW. The pulse durations applied were (from top to bottom) 2, 4, 6, 8 and 10 µs

The original substrate is shown in Fig. 4.5. It is apparent from this picture that no full removal of the film has taken place. The EDAX analyses revealed that the material remaining on the original support contained mainly yttrium from the metallic components. These areas when examining with optical microscope are fairly transparent and have a white-yellowish color which is characteristic for yttria (Y_2O_3).

Quantitative analyses by EDAX for the metallic constituents in the deposited stripes were performed for the whole regime investigated experimentally. All deposited stripes show Ba depletion and complete

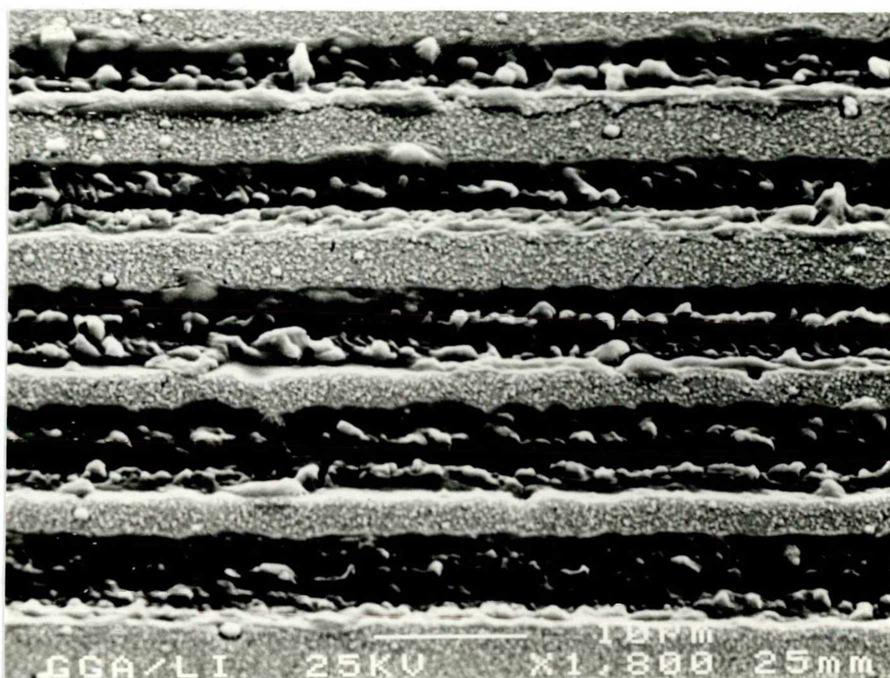

Fig. 4.5. The ablated areas processed by Ar^+ laser pulse series. The incident power was 779 mW. The pulse durations applied were (from top to bottom) 2, 4, 6, 8 and 10 μs

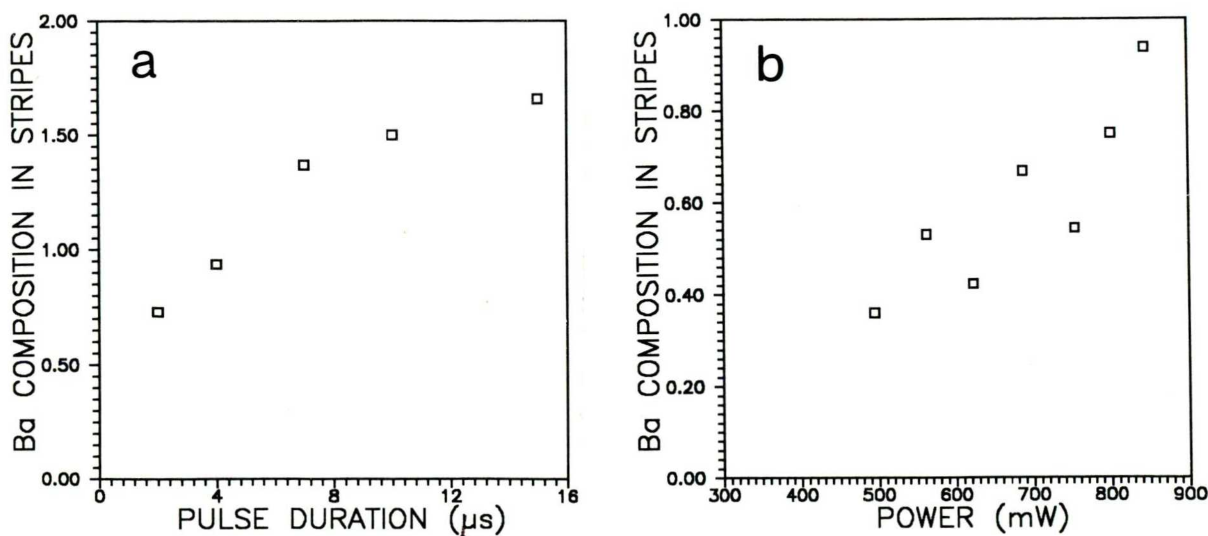

Fig. 4.6. Ba composition in stripes deposited from MgO support. a: The incident power was fixed at 846 mW, b: The pulse duration was kept on a constant value of 4 μs

lack of Y. In Figs 4.6.a and 4.6.b typical results of the quantitative analyses are shown. The ratio of the metallic components in the stoichiometric Y-Ba-Cu-O material is $N_Y:N_{Ba}:N_{Cu}=1:2:3$. On noting the depletion of Y and Ba in the stripes we compared the atomic numbers N_Y and N_{Ba} relative to the atomic number of copper N_{Cu} in such a way that the composition for Ba (x_{Ba}) and Y (x_Y) is represented by the ratio $N_Y:N_{Ba}:N_{Cu}=x_Y:x_{Ba}:3$.

Note that the Ba content is increasing both with the pulse duration and the processing power, but does not reach the optimum value of 2. Ba compositions closest to the value of 2 were measured in the stripes processed with high power and large pulse durations; this regime coincides with the regime of MgO removal.

4.3.2. Fused Silica Support

The results with MgO support outline the necessary conditions for stoichiometric LIFT. A faster heating rate is required to elevate the temperature up to a point where the components evaporate simultaneously. The high temperature need not melt/vapourize the support/substrate surface. Changing the support material from MgO to fused silica allows faster heating rates since the thermal conductivity of fused silica is much lower than that of MgO; consequently the formed temperature profile is much narrower. This feature is consistent with the observation that a scanning beam of 25 mW ($2w_0=3$ μm and $v_{scan}=3$ mm/s) proved to be sufficient to vapourize the 1 μm thick compound 123 layer. Deposition onto the MgO substrate commenced above 35 mW resulting in continuous well sticking lines and reproducing the morphology of the source film. Damage of the quartz surface could be detected by optical microscopy above 300 mW.

The results on processing 300 nm thick Y-Ba-Cu-O films on quartz support by pulse series are summarized in Figs. 4.7, 4.8 and 4.9. For all these results the scanning velocity, the beam diameter and the repetition rate were 50 μm/s, 3 μm and 40 Hz, respectively, so the factor of overlapping, O was the value of 2.4.

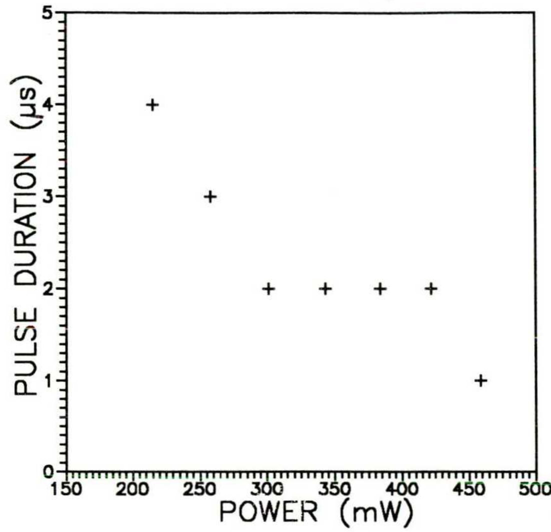

Fig. 4.7. Thresholds of the onset of continuous stripe formation (+). Support material: quartz.

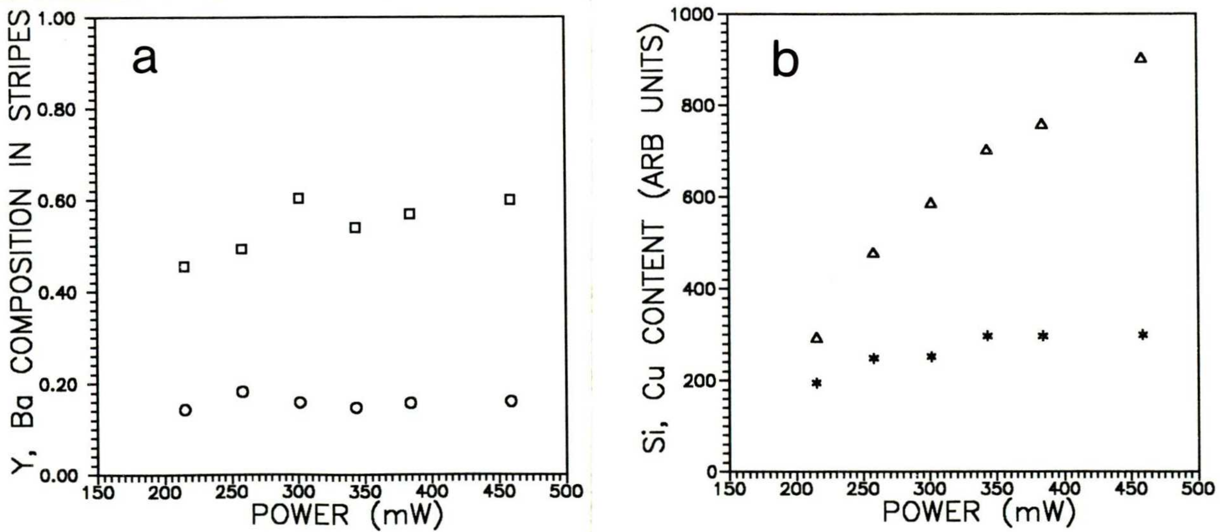

Fig. 4.8. a: Y (o) and Ba (□) composition and b: Si (Δ) and Cu (*) content in the stripes deposited from quartz support. Pulse duration was fixed at a value of 5 μs

In Fig. 4.7 the thresholds for continuous deposition are shown. The region for good quality deposition above the + signs is quite broad, the damage threshold for the quartz support being above power levels of ≥ 320 mW and pulse durations ≥ 10 μsec, respectively.

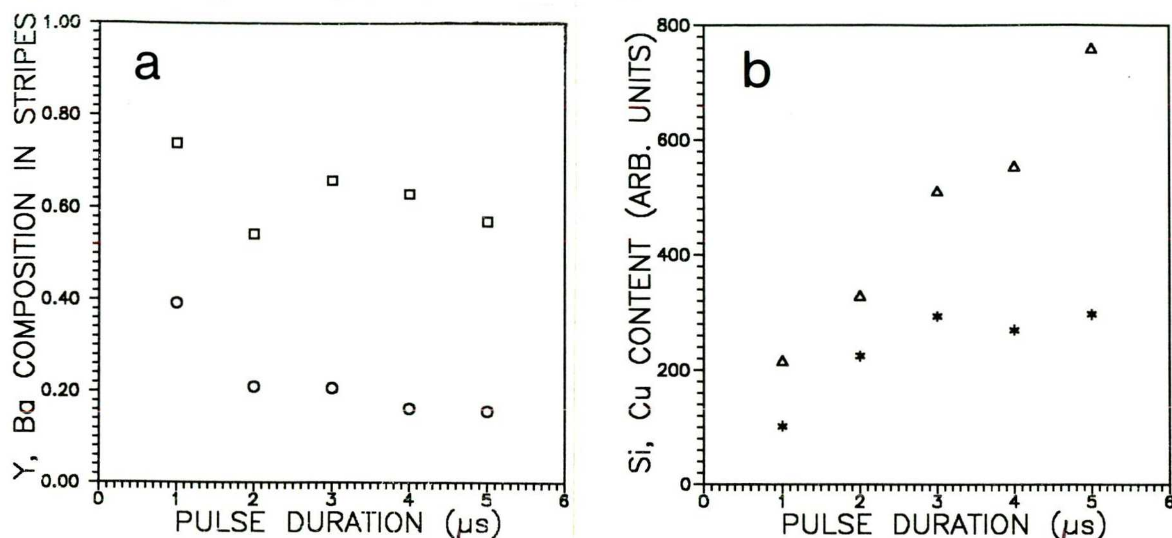

Fig. 4.9. a: Y (o) and Ba (□) composition and b: Si (Δ) and Cu (*) content in the stripes deposited from quartz support. The applied peak power: 384 mW

As expected in the stripes transferred from quartz Y was found as well. From Figs. 4.8.a and 4.9.a it is apparent that the processing power weakly influences the Y and Ba composition, however the pulse duration plays a more definitive role. The dependence of Y and Ba composition on the pulse duration is opposite to the dependence when transferring from MgO surface. In this case greater ratios of Y and Ba were observed when processing with smaller pulse durations. The morphological studies suggest that short pulse durations bring about material removal from the support surface in liquid phase since the deposits consist of small resolidified droplets (cf.: upper stripes in Figs. 4.10 and 4.11). For larger pulse durations evaporation sets on establishing contiguous deposit formation.

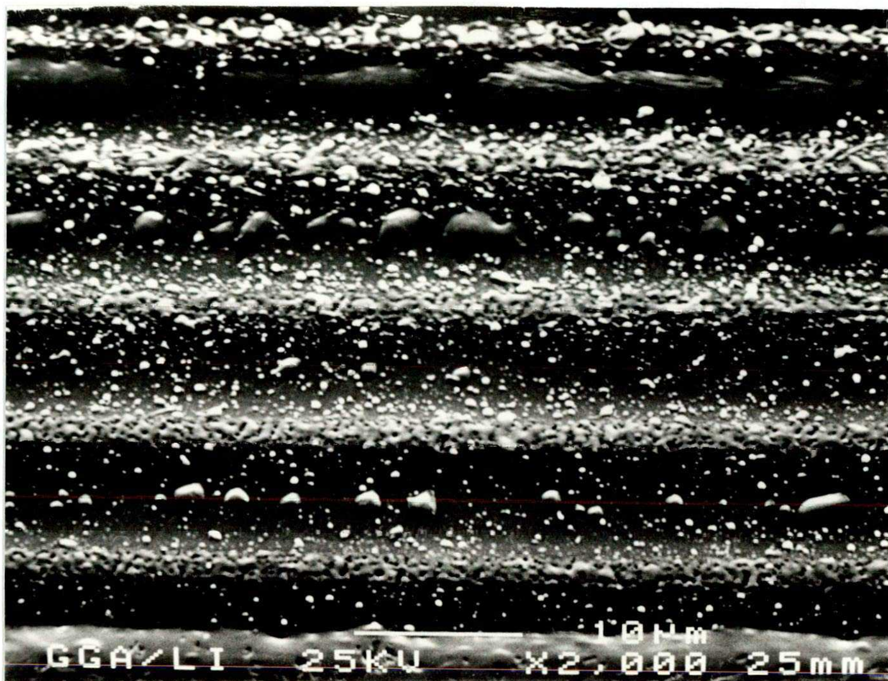

Fig. 4.10. Lines deposited by Ar^+ laser pulse series. The incident peak power was 384 mW. Pulse durations applied (from top to bottom) 1, 2, 3, 4 and 5 µs

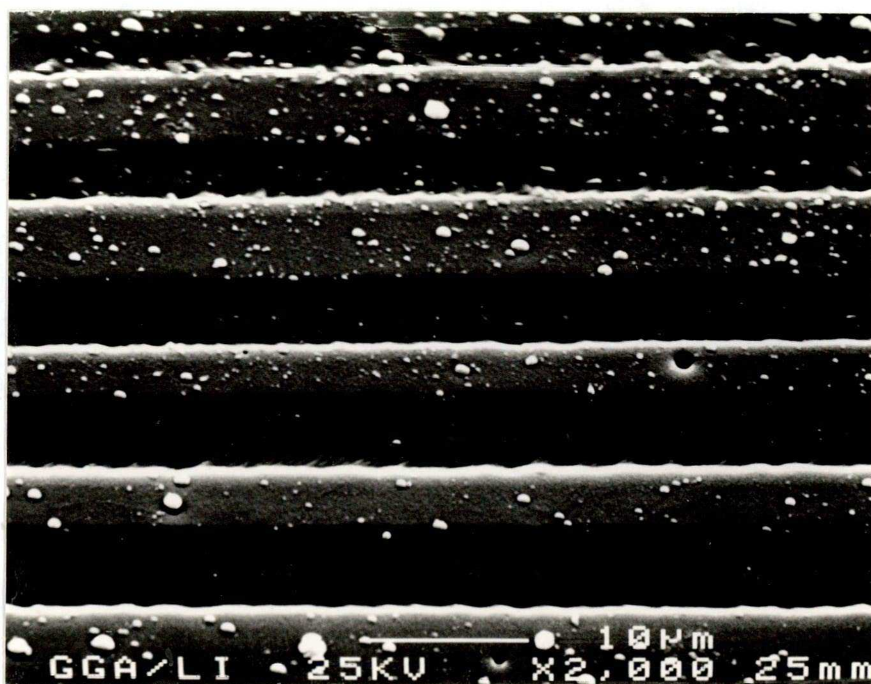

Fig. 4.11. The ablated areas processed by Ar^+ laser pulse series. The incident peak power was 384 mW. Pulse durations applied (from top to bottom) 1, 2, 3, 4 and 5 µs

In Figs 4.8.b and 4.9.b the changes in Cu and Si content of the stripes are shown. Although in this regime the damage of the quartz substrate is not apparent EDAX studies clearly indicate the presence of Si in the deposits, which vigorously increases with increasing power and pulse duration.

4.3.3. $SrTiO_3$ Support

The $SrTiO_3$ material has several common features with MgO and quartz. The adhesion of the films onto $SrTiO_3$ is extremely good, in fact, even better than onto MgO. From thermal point of wiew the thermal properties of $SrTiO_3$ are closer to that of quartz and so the results concerning $SrTiO_3$ support provide a more complete understanding as to the role of the thermal and adhering properties. In this case the scanning velocity, the beam diameter and the repetition rate were 235 μm/s, 6 μm and 200 Hz, respectively, so the factor of overlapping, O was the value of 5.1.

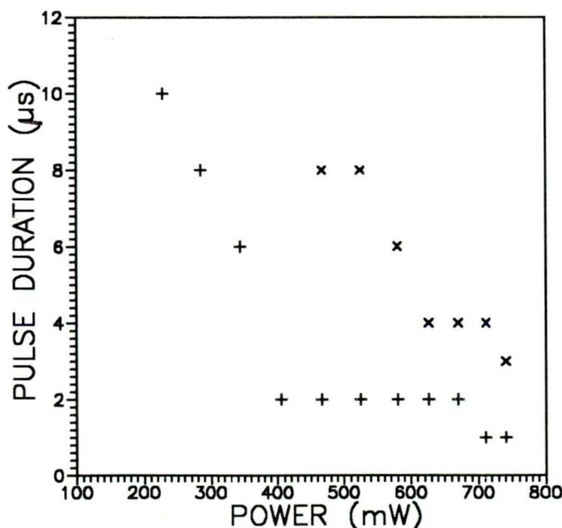

Fig. 4.12. Thresholds of the onset of continuous stripe formation (+) and damage/evaporation of the support material ($SrTiO_3$) (x). The area between + and x symbols represents the regime for deposition stripes of good morphology

In Fig. 4.12 the regime for good morphology deposition is illustrated. This regime is quite broad and reflects essentially the same characteristics as that observed in the case of quartz support.

Like in the case of MgO support no Y could be detected in the stripes although the trends for Ba composition (Fig. 4.13) gives the same behaviour as observed for quartz supports.

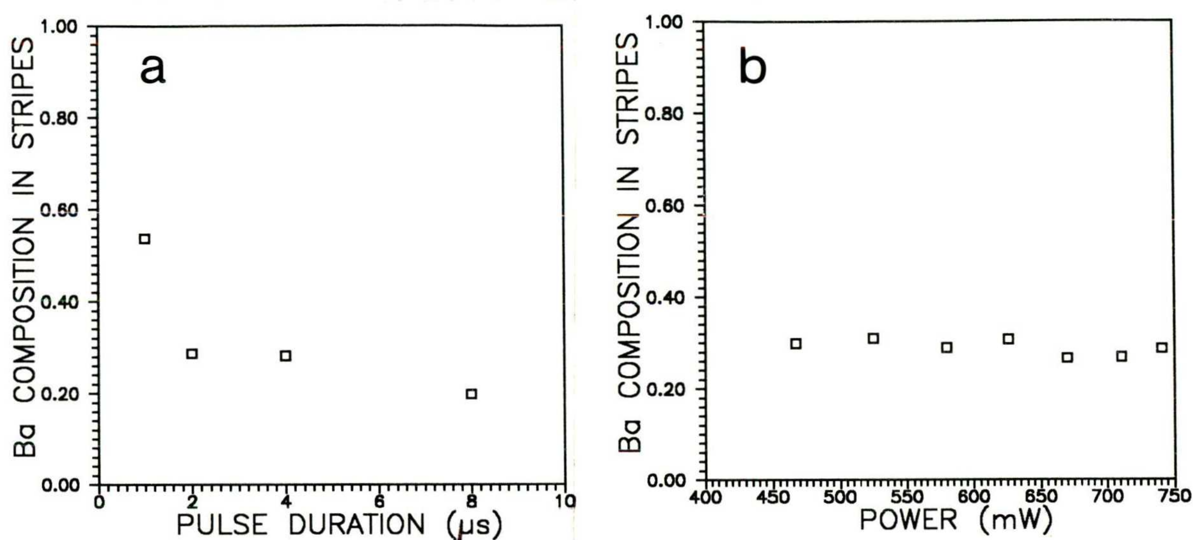

Fig. 4.13. Ba composition in stripes deposited from $SrTiO_3$ support. a: The incident power: 741 mW; b: The pulse duration: 2 μs

4.3.4. Discussion

The apparent Y and Ba depletion in the deposited films can be interpreted on the basis of the thermal properties of the oxide components. Above approx. 1000-1200 K phase separation for compound 123 ceramics is a characteristic event. On the basis of the melting and boiling temperatures of the constituting oxides the following sequence of evaporation can be anticipated. CuO decomposes at 1183K to Cu_2O and O, and Cu_2O melts at 1508 K and decomposes to liquid metallic

Cu (melting point of Cu is 1356 K) and O at ~1946 K, and finally Cu boils at 2840 K. The melting and boiling points of BaO are 2191 and ~ 2280 K, respectively. The highest melting point oxide is Y_2O_3 with a melting point of 2683 K and the vapor pressure reported by the manufacturer is essentially zero. The outgasing of species from compound 123 ceramics during low heating rate follows the order of Cu, BaO and Y_2O_3. When only the Y_2O_3 and BaO mixture remain on the support surface the heating of this remaining layer is rather ineffective since these compounds are transparent at the processing wavelength explaining the depletion of Ba and Y in the condensates.

The same non-stoichiometric behaviour is indicated in the literature for traditional evaporation methods. Terasaki et al. reported on electron beam deposition of Y-Ba-Cu-O films from stoichiometric sources [29]. They found that best stoichiometry could be reached when the source pellet was fully evaporated. Even in films prepared in such a way the composition was found to be $N_Y:N_{Ba}:N_{Cu}=0.25:1.66:3$. Hatou et. al. prepared superconducting films by flash evaporation which was carried out by dropping fine powder of stoichiometric 123 compound onto a heated W basket [30]. In the films about 6% W was detected and the metallic composition was found to be $N_Y:N_{Ba}:N_{Cu}=0.36:1.45:3$.

The experimental results given above outline the necessary conditions for stoichiometric LIFT. Let us consider for example the results obtained for quartz support. From Fig. 4.9. it is obvious that for producing greater amounts of Y and Ba in the deposits much smaller pulse duration is preferable. To obtain contiguous deposits greater power is required when using short pulse durations (c. f. Fig. 4.7). This leads to the problematics of the pulsed laser processing which

was discussed in Section 4.2.(page 36). An additional difficulty is the simultaneous evaporation of the support material and its subsequent mixing with compound 123 in the deposit layer as illustrated in Figs. 4.8.b and 4.9.b even when short laser pulses are used.

A few experiments have been made on the Bi-Sr-Ca-Cu-O system too. Similar problems with the stoichiometries emerged; the depletion of Ca and Sr was observed in large deposition parameter scales.

5.4. Conclusions

The implications of these results are twofold. First, very good quality patterns of higher spatial resolution and better characteristics can be obtained by using focused Ar^+ beam than ever reported in the literature for the LIFT technique. Second, both XeCl excimer and Ar^+laser induced forward transfer of compound 123 films is not expedient to obtain superconducting patterns since the requirements are not compatible with the possible processing conditions.

5. Pulsed Laser Processing of Bilayer Thin Film Structures

The synthesis of compound films by cw laser irradiation of alternating multiple layers of the elements is a challenging technique introduced by the Mons group. A great variety of polycrystalline films of good quality and surprisingly well defined stoichiometry (binaries and even ternaries) have already been produced by this simple process [31-37]. Continuous laser (i.e. low power) processing completely transforms the whole layer structure into compound preserving the initial composition predefined by the thickness of the elemental layers without material loss. The effects induced by high power pulsed laser irradiation of the same multilayer structures, on the other hand, are much more complex. Initial results on excimer [38] and ruby laser processing of Ge/Se bilayers [39] indicated selective etching or compound formation on the surface depending on the energy density and the sequence of the constituents.

Here we report the results of a systematic study on Q-switched ruby laser processing of supported Ge/Se structures. We made the first systematic study of the LIFT technique for depositing from bilayers while initiating chemical reaction between the constituents. Providing transfer and mixing/compound formation can be coupled resulting in compound print formation from multilayer structures it is a great promise to produce compound semiconductor patterns in a given stoichiometry by a simple single step deposition technique.

5.1 Experimental

The bilayer structures consisting of 74nm Se and 30nm Ge (Se:Ge atomic ratio = 2:1) were vacuum evaporated onto cleaned glass and NaCl supports in both sequences. For a comparison Se and Ge monolayers were evaporated onto glass with the same thicknesses as in the bilayers. In order to pick up the material removed and to monitor the efficiency of the transfer a blank substrate (glass or NaCl) was placed in contact with the mono- and bilayer structures. These samples were irradiated through a mask from both directions (Fig.5.1: front side and back side illumination) through the optical setup described in section 3.1.1. The energy density impinging on the sample surface Φ_{inc} was tuned in steps of min. 10 mJ/cm^2 between 0 and 2 J/cm^2 using homogenizers of different aperture and calibrated filters. The transmittance T and reflectance R of the samples was measured in all four configurations (Fig. 5.1) prior to processing. Since the reflectances were significantly different for different configurations in order to be able to compare the events for the different side illuminations the effective fluence absorbed in the bilayer was defined by the expression $\Phi_{abs}=\Phi_{inc}(1-R-T)$ and correlated with the different events. The calculation of Φ_{abs} by this way gives coarse estimates since both transmittance and reflectance can vary rather significantly during processing.

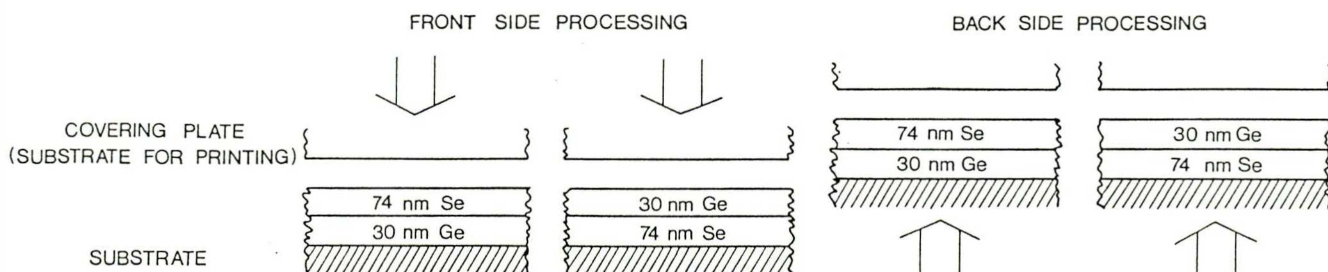

Fig. 5.1. Se/Ge bilayer sample configurations

Morphological changes in the processed areas and in the deposits were analyzed by optical and electron microscopy (TEM, ED, SEM), while changes in chemical composition were followed by X-ray microanalysis (EDAX) and optical spectroscopy in the visible and near IR.

5.2. Pulsed Laser Processing of Ge/Se Bilayer Structures

Comparative studies on samples of processed areas of different shape and sizes ranging from 1 to 100 mm^2 revealed that the characteristic properties of the films both on the support and the substrate were independent of the lateral dimensions. The morphology and chemical composition of both the remaining layers and the prints are determined by the sequence of the elemental layers and the absorbed fluence. Both transformed areas and prints are sharp reproductions of the mask window. Processing in air and vacuum resulted in amorphous films of virtually identical properties within the detection limits of our analytical methods.

Since the absorption coefficients of selenium and the glass substrate are more than three orders of magnitude lower than that of germanium at λ=694 nm [41, 42] practically the whole energy of the processing ruby laser pulse is absorbed in the Ge leading to a local heating of this layer predominantly. Since the thermal conductivity of Ge is relatively high the temperature within the whole layer is practically uniform. As the temperature calculations revealed the maximum temperature difference between the top and bottom of that layer was <20 K for the highest fluence used. The adjacent layer(s) are heated dominantly by the heat flow from the hot Ge layer. In the Se a very high temperature gradient may build up as the thermal

conductivity of this material is even lower than that of the glass. Since the melting (490K) and boiling point (958K) of Se is lower than the melting point of the Ge (1210K) a characteristic feature of the Ge/Se system is the coexistence of different phases: with raising temperature a small portion of Se melts and then boils at and near to the Se-Ge interface while the Ge layer remains in the solid phase. This is exemplified by the temperature distributions shown in Fig. 5.2 which have been calculated for both layer sequences using the same fluence. As shown in Fig. 5.2b at the moment when the Ge layer melts a large amount of vaporized and molten Se is present. In the case of the

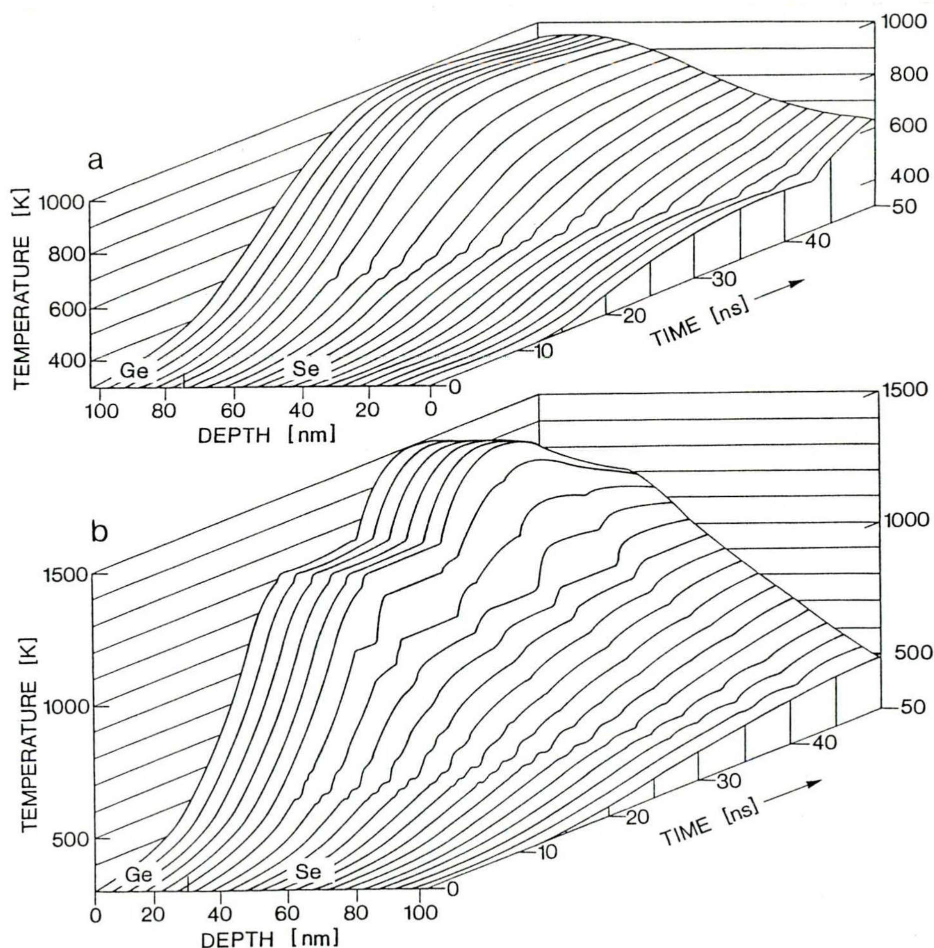

Fig. 5.2. Calculated temperature distributions for Φ_{abs}=30 mJ/cm. Sequences: a) substrate-Ge-Se-cover and b) substrate-Se-Ge-cover

substrate-Se-Ge-(air)-cover sequence the temperature in the Ge layer raises faster and attains a higher value than in the case of the reversed sequence since the dominant heat flow is towards one side in the former and both sides in the latter case. (As the thermal parameters of the encapsulated Se vapour are unknown we extrapolated data corresponding to lower temperatures for the model calculations. Consequently the calculated quantities given below for the Se vapour thicknesses are order of magnitude estimates and will be used for relative comparison only.)

5.2.1. Glass-Se-Ge Layer Sequence

Having Ge as the top layer (support-Se-Ge -substrate sequence) the front and back side illumination result in the same events characterized by the same absorbed fluence thresholds and material properties. No visible changes can be observed until the absorbed fluence is less than 15 mJ/cm^2. Just above this sharp threshold ablation of the whole Ge layer starts without visible changes in the underlying Se layer. The ablated germanium appears in form of chips on the cover plate. On increasing the fluence the Ge chips change into molten fragments sticking better on the cover surface. Above Φ_{abs}=25 mJ/cm^2 the deposits consist of 0.4-0.8 μm diameter resolidified droplets distributed homogeneously on the cover plate providing evidence for the melting of the whole germanium layer. This morphology results in practically constant transmittance and reflectance in the whole visible and near IR, i.e. the prints behave as grey optical filters. As shown in Fig. 5.3 the thickness of the Se films remaining on the substrate after Ge ablation (measured by comparing the absorption of these to that of a reference Se layer of known

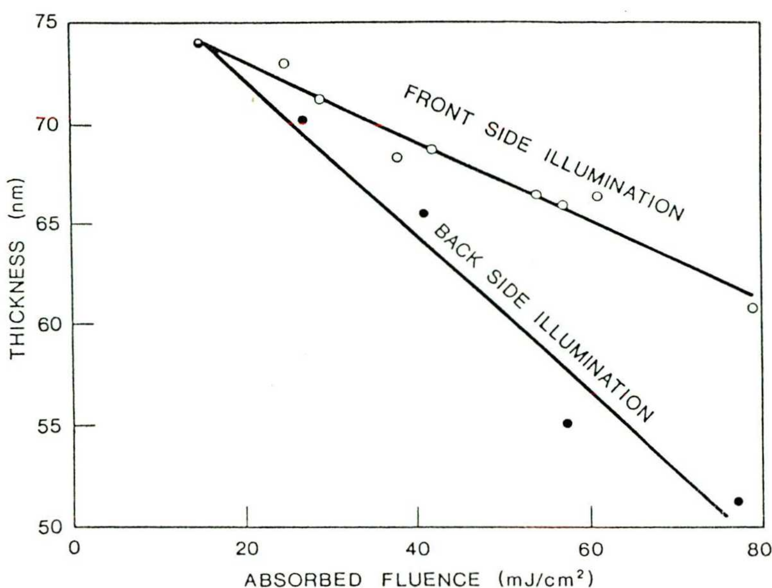

Fig. 5.3. Measured thickness of the Se layer remained on the substrate after Ge ablation as a function of absorbed fluence for front side (o) and back side (•) illumination. Sequence: substrate-Se-Ge-cover

thickness) decreases with increasing energy density between 15 and 90 mJ/cm^2. The removal of selenium from the original substrate is substantiated by the appearance of Se deposit on the cover plate as confirmed by electron microscopy and X-ray microanalysis. Above $\Phi_{abs}=55$ mJ/cm^2 the prints consist of tiny Ge droplets covered by a continuous Se layer. The corresponding absorption spectra are superpositions of the grey filter and Se spectra.

At fluences $\Phi_{abs} \cong 90$ mJ/cm^2 an unexpected effect emerges: less and less Ge can be ablated from the top of Se layer as apparent from the decreasing amount of Ge transferred onto the cover. If the absorbed energy density becomes higher than approx. 180 mJ/cm^2 the color of the processed area turns into yellowish indicating the onset of compound formation on the support. This process proceeds with negligible material loss. Optical spectroscopy and EDAX analyses verified that the Ge:Se atomic ratio in the formed compound film was near to 1:2,

i.e. the original composition defined by the thickness of the elemental layers. On further increasing the fluence the dominant process remains compound formation on the support accompanied by the appearance of increasing amount of compound on the cover substrate.

For the support-Se-Ge-cover configuration our temperature profile calculations show that Ge melting starts at approx. 20 mJ/cm^2 and the Ge layer melts throughout at $\Phi_{abs} \cong 25$ mJ/cm^2. Se vaporization starts at significantly lower fluences: above $\Phi_{abs}=9$ mJ/cm^2 a thin Se vapour layer emerges at the Se-Ge interface. The Ge ablation threshold observed experimentally lies at $\Phi_{abs}=15$ mJ/cm^2. To the fluence domains limited by these three threshold values different approximations apply. Below 9 mJ/cm^2 the calculated temperature distributions are obviously correct. Between Se vaporization and Ge ablation the model

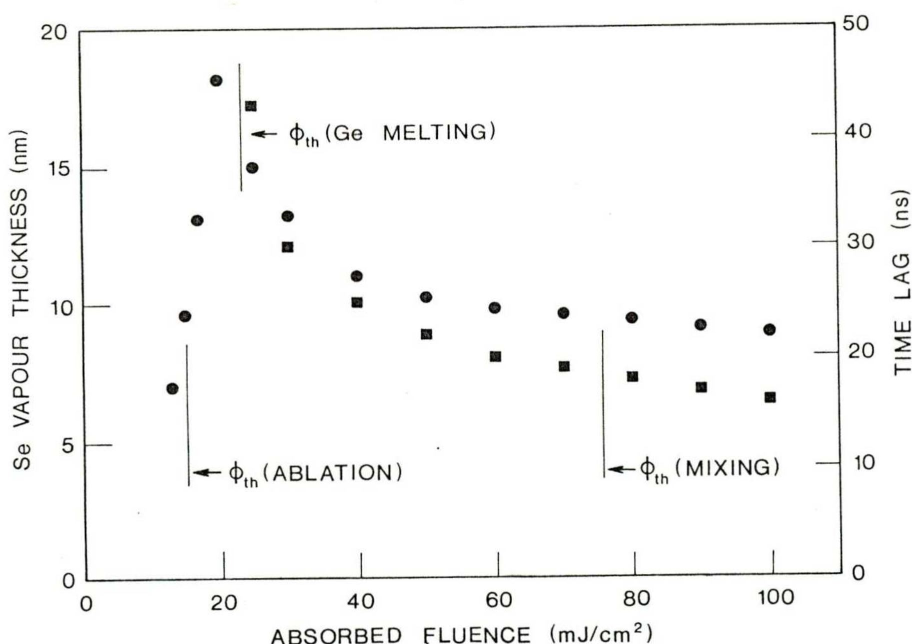

Fig. 5.4. Calculated Se vapour thicknesses (●) and - above 25 mJ/cm^2 - the time lag (■) between the beginning of the laser pulse and the melt-through of the whole Ge layer as a function of absorbed fluence. Sequence: substrate-Se-Ge-cover

yields a real estimate for the thickness of the Se vapour layer encapsulated below the solid Ge. Having no data on the time evolution of Ge ablation between 15 and 25 mJ/cm^2 the results of the model calculation are adequate to reflect the trends only. Above ≈ 25 mJ/cm^2 the whole Ge layer melts throughout during the laser pulse. The Se vapour thickness values calculated for fluences above Φ_{abs}=25 mJ/cm^2 refer to thicknesses built up until Ge melt-through.

In Fig. 5.4 calculated Se vapour thicknesses and, above 25 mJ/cm^2, the time lag between the beginning of the laser pulse and the melt-through of the whole Ge layer are plotted as a function of absorbed fluence. In the fluence range of 9-25mJ/cm^2 the solid Se layer thins down with progressing vaporization. Above a critical vapour pressure the enclosed vapour will blow off the top solid Ge layer. As shown in Fig. 5.4 the experimental ablation threshold Φ_{abs}=15 mJ/cm^2 corresponds to a calculated Se vapour thickness of ≈ 9 nm. At a fluence of ≈ 25 mJ/cm^2 the Ge layer is melted throughout only after blow off since the estimated thickness of the Se vapour layer is 15 nm which exceeds the critical thickness for blow off of 9 nm. With increasing fluence the melting of Ge requires shorter time periods: the time lag decreases. Therefore less and less Se can be vaporized until the complete melting of Ge. Above Φ_{abs}≅70-80 mJ/cm^2 the Ge melting is so fast (<17 ns) that the thickness of the Se vapour layer falls below the critical value of 9 nm and so the vapour pressure will not be sufficiently high for blowing off Ge in solid state. This fluence value well fits to the experimental results: above Φ_{abs}≅90 mJ/cm^2 a less complete Ge transfer is observed. It is clear from the calculations that using higher fluences the melting process is practically instantaneous; the probability of the synthesis rapidly

increases as the diffusion of the constituents is orders of magnitude higher in the liquid phase than in the solid.

Note that this behaviour well corresponds to the effect observed for metal LIFT; the melting usually hampers the effectivity of ablation from the support.

With the above approximations the rather obvious difference in Se removal between front and back side illumination cannot be explained. As seen in Fig. 5.3 the remaining Se layer becomes much thinner in the case of back side illumination than in the case of front side illumination. This effect can be incorporated into our model assuming that the absorption of Se for the ruby laser light is higher than expected and, thus, the energy absorbed by this layer will depend whether illuminated via the transparent substrate or the strongly absorbing Ge layer. When enhanced light absorption in the Se is also taken into account higher temperature and hence faster evaporation is expected in that layer for back side illumination than for front side illumination. To check this explanation we have processed a supported single Se layer of the same thickness as for the bilayer samples. Our experiments revealed that above $\Phi_{inc} \approx 600$ mJ/cm^2 Se pieces were removed from the sample and deposited on the cover. $\Phi_{inc} \approx 800$ mJ/cm^2 proved to be enough to melt the Se and form a more or less continuous layer on the cover. For these fluences temperature profile calculations indicate no significant heating when using the absorption coefficient given in Table A1 (p. 71). This disagreement emphasizes the role of Se absorption for the fluences used in the experiments.

5.2.2. Glass-Ge-Se Layer Sequence

In the case of samples of reversed layer sequence (support-Ge-Se

-substrate) front side and back side illumination result in different series of events with slight variances in energy density thresholds and material properties.

A characteristic series of photographs taken from areas processed by single pulses of increasing fluence and the corresponding deposits is shown for front and back side illumination in Fig. 5.5 and 5.6, respectively. The first threshold in the case of front side illumination is at Φ_{abs}=50 mJ/cm^2. Effective fluences between 50 and 80 mJ/cm^2 induce melting and partial removal of selenium leaving the underlying germanium layer undamaged. The SEM + EDAX analyses clearly show that in the remaining films resolidified Se islands are dispersed on the intact Ge surface while the deposits on the substrate consist of practically pure selenium in form of splashes of 5-10 μm diameter. With increasing fluence more and more Se leaves the surface and arrives at the substrate forming finally a continuous layer on it.

The threshold for back side illumination is somewhat lower at Φ_{abs}=43 mJ/cm^2. Slightly above this fluence Se and Ge fragments together leave the bilayer structure and stick to the substrate. The remaining layers consist of irregular Ge and Se islands, while on the substrate face 10-20 μm Se splashes and - in much less amount - 0.5-1 μm Ge droplets are dispersed. A typical scanning electron micrograph of a print deposited in this fluence range is shown in Fig. 5.7. The inhomogeneous structure results in practically constant transmittance and reflectance. As shown in Fig. 5.8 both the remaining layers and the prints possess essentially the same reflectance but slightly different transmittances due to the different amount of material present.

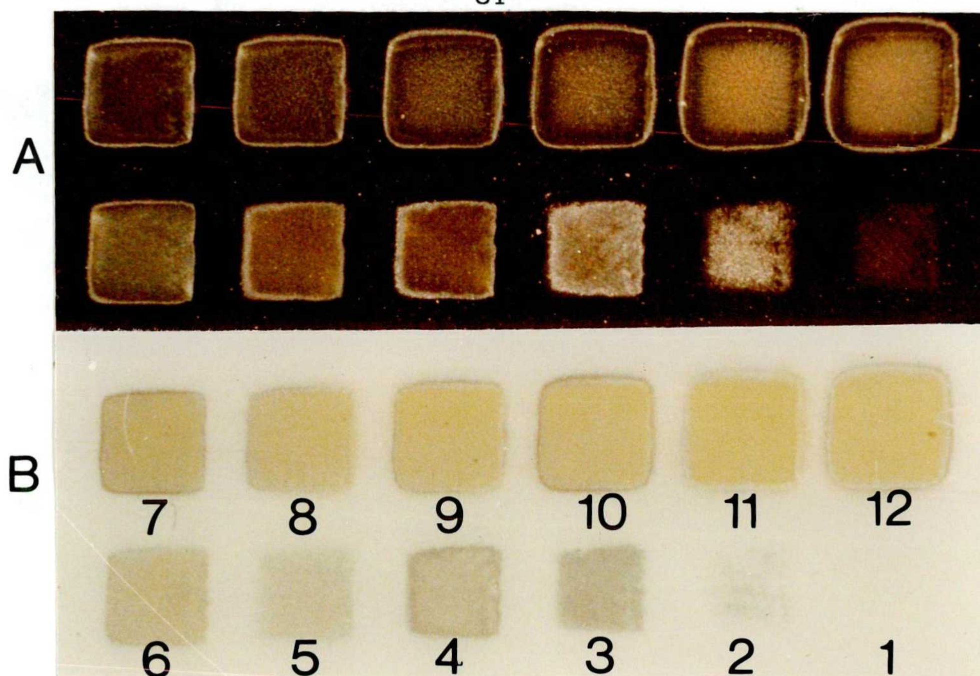

Fig. 5.5. Photographs taken from processed areas (A) and the corresponding prints (B). Layer sequence: substrate-Ge-Se-cover. Front side illumination. Absorbed fluences in mJ/cm^2: 1: 41, 2: 56, 3: 78, 4: 103, 5: 128, 6: 177, 7: 256, 8: 320, 9: 480, 10: 633, 11: 853, 12: 1115

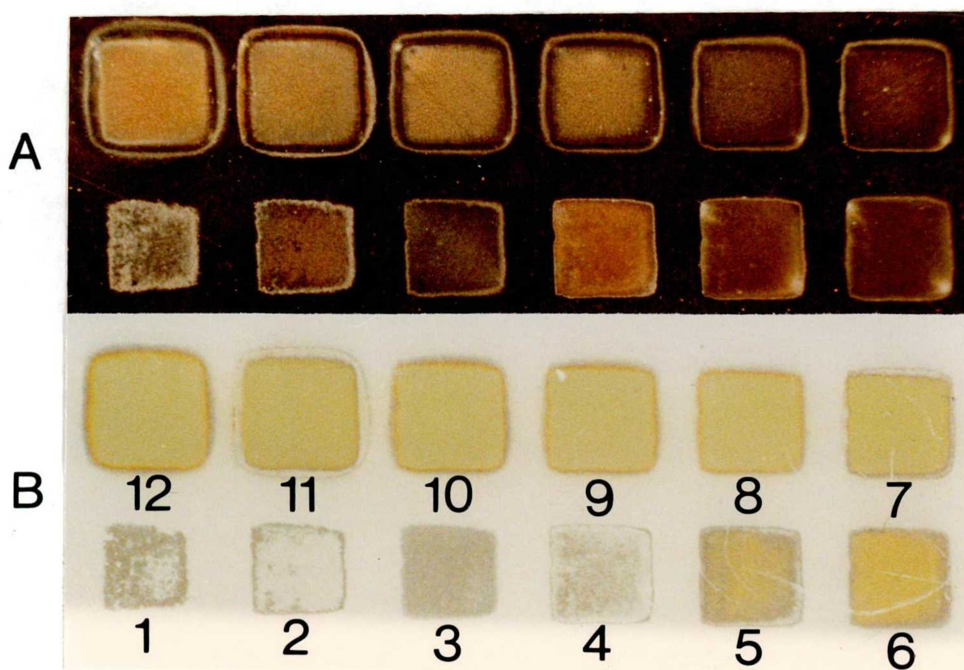

Fig. 5.6. Photographs taken from processed areas (A) and the corresponding prints (B). Layer sequence: substrate-Ge-Se-cover. Back side illumination. Absorbed fluences in mJ/cm^2: 1: 77, 2: 98, 3: 123, 4: 175, 5: 229, 6: 284, 7: 382, 8: 464, 9: 710, 10: 938, 11: 1519, 12: 1749

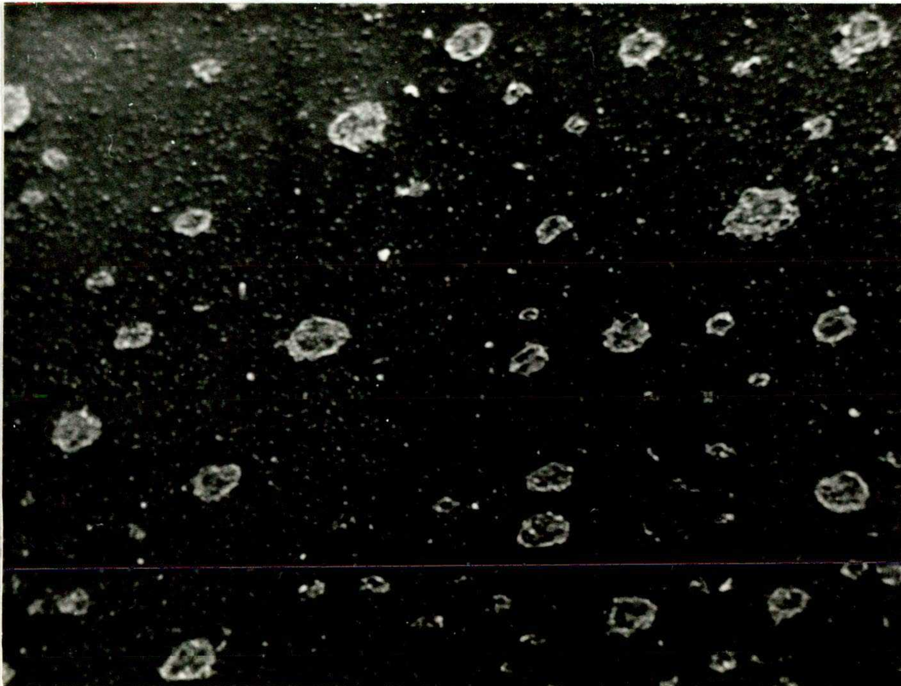

Fig. 5.7. Scanning electron micrograph of a print deposited at Φ_{abs}=93 mJ/cm^2. Sequence: substrate-Ge-Se-cover. Back side illumination. Enlargement: 500x

Processing at higher fluences results in the same sequence of events for both directions of illumination with no differences in morphology of the remaining layers and the deposits. Single pulses of fluences above $\Phi_{abs} \cong$ 80 mJ/cm^2 for front side and $\Phi_{abs} \cong$100 mJ/cm^2 for back side processing are sufficient for initiation of compound synthesis on the support while the deposits consist of a pure Se layer with small Ge droplets on it. With increasing energy density the Ge content in the prints gradually decreases up to $\Phi_{abs} \approx$ 170 mJ/cm^2. In the 170< Φ_{abs} < 200 mJ/cm^2 domain practically no Ge has been found on the cover plates. A further increase in the processing fluence leads to more and more complete mixing of the two constituents as reflected by the appearance of compound films on both substrates.

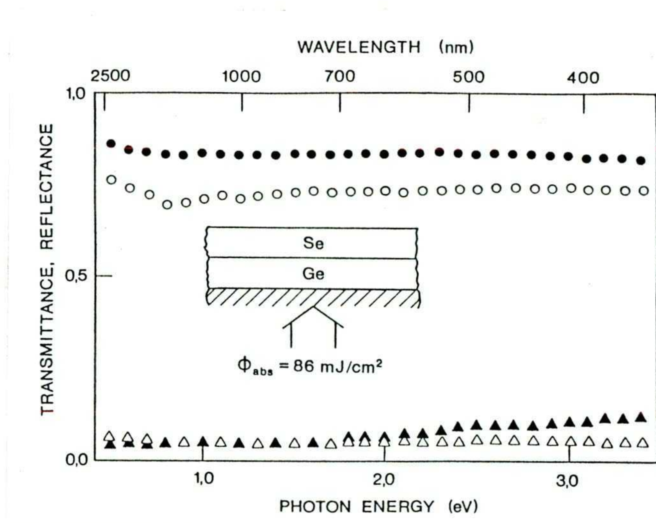

Fig. 5.8. Transmission (o) and reflection (Δ) spectra of a remaining layer and those of the corresponding print (●, ▲) processed with Φ_{abs} =86 mJ/cm^2

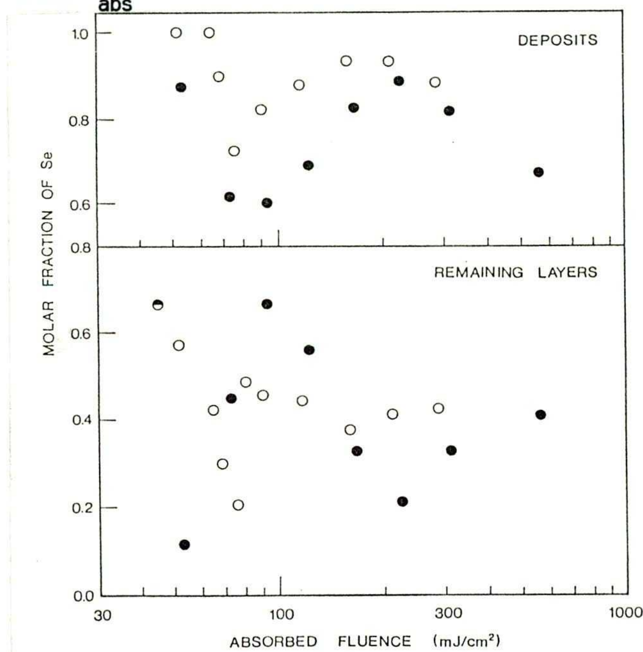

Fig. 5.9. Changes in chemical composition of the remaining layers and the prints as a function of absorbed fluence as determined by EDAX. o: front side illumination ●: back side illumination

Changes in the chemical compositions of the remaining layers and the deposits as a function of absorbed fluence are displayed in Fig. 5.9. Since the deposits are generally much thinner than the remaining layers it is an inherent feature of this technique that the removal of

small amounts of material from the bilayer and transfer to the cover plate may produce great alterations in the composition of the prints while leading to minor changes in the Se:Ge ratio in the remaining layers. Apparently the analysis of the prints is an excellent diagnostic tool as the changes appear in an enlarged scale.

The results of the elemental analysis correlate very well with that of the morphological analysis presented above. In the case of front side illumination (open circles in Fig. 5.9) the molar fraction of Se in the remaining layers first decreases with increasing fluence from the initial value of 0.66 down to ≈0.2 while this fraction approaches the value of 0.91 in the corresponding deposits indicating that the characteristic feature is indeed selenium removal from the support. At around 80 mJ/cm^2 there is a jump in both plots. Above this fluence the Se content in the remaining layers varies in the neighbourhood of 0.5 (equiatomic composition, GeSe) with a small local minimum at around $\Phi_{abs} \approx 160$ mJ/cm^2 while maximum values approaching 0.94 correspond to this minimum in the prints. For back side processing (closed symbols) the changes in the molar fraction of Se reflect essentially the same sequence of events with minor shifts in thresholds. The break in the plots appears at around 100 mJ/cm^2. Processing with fluences above this value leads to a steep decrease in the Se content of the remaining layers with a concomitant initial increase in that of the prints. Between 200 and 300 mJ/cm^2 a local minimum and maximum is observed in the remaining layers and in the prints, respectively, and after that the atomic ratios reach steady state values.

In the case of support-Ge-Se-cover sequence there is a heat exchange between the laser heated Ge layer and the adjacent layers via

the substrate-Ge and Ge-Se interfaces where great temperature gradients are formed. The events at the former play an important role in the initiation of Ge ablation while those at the latter govern Se removal and/or compound formation. As discussed above in paragraph 5.2.1. the absorption in the Se layer is not negligible for the high fluences applied and so the temperature profiles induced by front and back side illuminations differ significantly. In the latter case the laser pulse heats directly the substrate-Ge interface and so the temperature is higher than in the case of front side illumination when the light is attenuated in the Se layer before reaching the Ge layer. The higher temperature formed at the substrate-Ge interface is able to overcome the temperature limit for ablation in the case of back side illumination while in the case of front side processing the same fluence results in temperatures below this limit. The same effect accounts for the slight variances in the first thresholds ($\Delta\Phi$=5 mJ/cm^2) and different events.

Taking into account the role of the Se-Ge interface it is easy to understand why partial ablation and transfer of Se is detected in a wide fluence range. Temperature calculations show that above $\Phi_{abs}\cong30$ mJ/cm^2 vaporization starts at the bottom of the Se close to the unmelted Ge as indicated in Fig. 5.10. At the ablation threshold Φ_{abs}=45 mJ/cm^2 the calculated thickness of the Se vapour layer is already ≈ 11.4 nm, the central part is molten and the top adjacent to air remains solid. In this fluence domain the Se vapour blows off the upper molten and solid Se. The ablation is never complete since a certain part of molten Se remains on top of the Ge layer. With increasing fluence more Se is vaporized so the efficiency of Se removal is increasing. The model calculations indicate the melting of

the Ge at the fluence of Φ_{abs}≈60 mJ/cm^2. Similarly for Fig. 5.4 the time lag between the melting of Ge and the start of laser pulse is plotted in Fig. 5.10 and above 60 mJ/cm^2 the calculated Se vapour

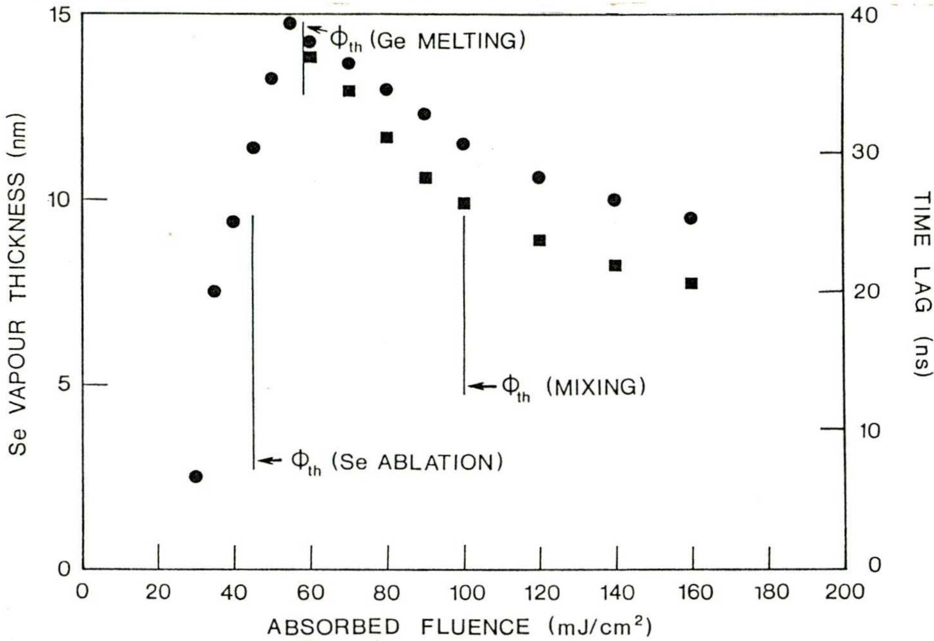

Fig.5.10. Calculated Se vapour thicknesses (●) and - above 60 mJ/cm^2 - the time lag (■) between the beginning of the laser pulse and the melt-through of the whole Ge layer as a function of absorbed fluence. Sequence: substrate-Ge-Se-cover

thicknesses refer to the appropriate time lags. When Ge melting commences earlier than Se blowing off occurs the mixing and synthesis of the remaining Se and the molten Ge starts as described for the opposite layer sequence. The thickness of calculated Se vapour falls below the critical value of 11.4 at about Φ_{abs}≈100 mJ/cm^2 which well corresponds to the experimental threshold of mixing. With increasing fluence practically no Ge is transferred to the cover which accounts for the high Se:Ge ratios in the prints.

Above a fluence of Φ_{abs}=160-200 mJ/cm^2 the temperature increases very steeply in the bilayer and within a few nanoseconds both Ge and Se is melted or vaporized. In this regime the evolution of the

processes can be estimated from the experimental results only. Obviously the mixing of the elements on both plates is better for higher fluence processing. This trend is clear from Fig. 5.9. A better mixing alters the proportions of the elements on the original substrate to Ge:Se=1:1 and on the cover to Ge:Se=1:2 at the highest fluences used. Both the remaining layers and the prints are homogeneous, continuous and smooth revealing that pulsed ruby laser processing at adequate fluences is appropriate to form well defined and good quality compound patterns of chemical composition close to GeSe and $GeSe_2$ both on the support and the covering substrate, respectively.

5.3. Conclusions

The comparison between the presented experimental data on pulsed laser processing of Ge/Se bilayer structures and calculated temperature distributions enabled us to unfold the rather complicated events into elementary steps. The characteristic processes are selective transfer of one of the constituents, compound formation on the original substrate and simultaneous transfer of the preformed compound. The morphology and chemical composition of both the remaining layers and the prints depend on the sequence of the elementary layers and the absorbed fluence Φ_{abs}. The processes are initiated by a temperature rise due to the absorption of the laser light; the temperature profile calculations give valuable information on the details of the events. The striking agreement between experimental findings and model calculations indicates the validity of the simple thermal model applied.

From technological point of view our procedure has established a novel, inherently simple, single-step-technique for local deposition of compound films from stacked elemental layers on a transparent support as a source onto any target surface.

6. Summary

Our comparative study on Q-switched ruby laser (λ=694 nm, $h\nu$=1.79 eV, 20 ns FWHM) processing of supported vanadium, titanium and chromium thin films and Ge/Se multilayer structures give a very detailed insight into the advantages and limitations of this method. Since lateral resolution and morphology/quality of the prints are of critical features in future applications, we concentrated on the role of the glass support-film interface in determining the characteristics of ablation kinetics and subsequent printing, and on the dependence of the morphology and lateral dimensions of transferred patterns on target-source distance [9, 43].

We analyzed the kinetics of the subsequent steps, namely ablation of the metallic monolayers; mixing and/or partial ablation of the multilayer structures by comparing experimental data with calculated temperature distributions in space and time [8, 9, 39, 40, 43, 44].

In the case of poorly adhering films the transfer yield is independent of film-to-substrate distance between 0 and 60 μm throughout the fluence range studied. The transmittance of the ablated areas of well adhering films decreases and that of the corresponding prints increases with increasing distance as evaporation becomes dominant [8, 9, 43].

Our results revealed that the description of the mechanism of LIFT given by Bohandy and coworkers [3-6] is oversimplified: The driving force for propulsion can be explained by interfacial effects and so LIFT can be realized with fluences which are not sufficient to melt the target and still result ablation in solid phase. The

target-to-substrate distance plays an essential role in determining the quality of transfer [8, 9, 43].

By using Ge/Se multilayer structures as targets we could deposit even non absorbing Se layers applying the LIFT technique. We established a novel, inherently simple, single step technique for synthesizing and transferring compound films from stacked elemental layers as targets onto any substrate with a single laser pulse [39, 40, 44].

The LIFT by means of scanning cw laser beam was demonstrated; homogeneous continuous lines could succesfully be deposited with the best lateral resolution (2-3 μm wide stripes) ever reported in the LIFT literature. We obtained that the LIFT of high critical temperature Y-Ba-Cu-O ceramics has no perspective since the requirements to obtain superconducting patterns do not coincide with the possible LIFT circumstances.

The transfer of thin films from a (transparent) support onto another substrate in close proximity with one single laser pulse or by a scanning laser beam is an attractive and simple novel approach to surface patterning. (i) The properties of the surface to be patterned have no effect either on the process or the quality of the print, i.e. any substrate can be patterned using this method. (ii) It can be performed in air; there is no need for expensive gas handling/vacuum systems. (iii) This technique offers the unique possibility of depositing compound films by mixing and transferring the constituents from supported multilayer structures as sources in a single step. (iv) High lateral resolution can be reached which fulfils the requirements of the advanced microtechnologies.

Table A.1. Thermal and optical data of the materials used [22, 23]

	Ti	Cr	Se	Ge	Glass
Melting point [K]	1941	2148	490.2	1210	-
Boiling point [K]	3533	2938	958	3103	-
Latent heat of melting [Jkg^{-1}]	$3.23 \cdot 10^5$	$2.66 \cdot 10^5$	$6.86 \cdot 10^4$	$4.79 \cdot 10^5$	-
Latent heat of boiling [Jkg^{-1}]	$9.31 \cdot 10^6$	$5.87 \cdot 10^6$	$7.57 \cdot 10^5$	$3.92 \cdot 10^6$	-
Density [kgm^{-3}]	$4.51 \cdot 10^3$	$7.19 \cdot 10^3$	$4.28 \cdot 10^3$	$5.32 \cdot 10^3$	$2.55 \cdot 10^3$
Thermal conductivity [$Wm^{-1}K^{-1}$]	$-1.27 \cdot 10^{-9}T^3$ $+8.09 \cdot 10^{-6}T^2$ $-8.37 \cdot 10^{-3}T$ $+22.72$	$-3.01 \cdot 10^{-9}T^3$ $+2.40 \cdot 10^{-5}T^2$ $-6.08 \cdot 10^{-2}T$ $+106.92$	$-1.7 \cdot 10^{-5}T^2$ $+1.4 \cdot 10^{-2}T-$ -2.52 $T<490K$ 0.25 $T>=490K$	$-2.7 \cdot 10^{-8}T^3+$ $+1.14 \cdot 10^{-4}T^2-$ $-0.157T+80$	$1.8 \cdot 10^{-3}T+0.6$ ($T<1000K$) $1.8 \cdot 10^{-4}T^2$ $-0.362T+182.5$ ($T>1000K$)
Specific heat [$Jkg^{-1}K^{-1}$]	$0.18T+479$	$0.24T+399$	$0.23T+251$	$6.5 \cdot 10^{-2}T+340$	$0.27T+587$
Absorption coefficient [m^{-1}]	$7.1 \cdot 10^7$	$9.2 \cdot 10^7$	$1.1 \cdot 10^4$	$3.63 \cdot 10^7$ *	-
Reflection coefficient	0.31	0.41			-

REFERENCES

1. D. Bäuerle: Chemical Processing with Lasers, Springer Series in Materials Science 1. (Springer, Berlin - Heidelberg - New York) 1986.

2. V. P. Veiko: Lazernaya abrabotka pl'onochnih elementov (Izdatel'stvo, Leningrad 1986) p. 148

3. J. Bohandy, B. F. Kim, F. J. Adrian: J. Appl. Phys. **60**, 1538 (1986)

4. F. J. Adrian, J. Bohandy, B. F. Kim, A. N. Jette: J. Vac. Sci. Technol. B **5**, 1490 (1987)

5. J. Bohandy, B. F. Kim, F. J. Adrian, A. N. Jette: J. Appl. Phys. **63**, 1158 (1988)

6. E. Fogarassy, C. Fuchs, F. Kerherve, G. Hauchecorne and J. Perriere, J. Mater. Res. **4** (5), 1082, (1989)

7. R. J. Baseman, A. Gupta, R. C. Sausa and C. Progler, *Laser and Particle-Beam Chemical Processing for Microelectronics*, Proc. MRS 101, Ed. by D. J. Ehrlich, G. S. Higashi, M. M. Oprysko (MRS, Pittsburgh, PA 1988) p. 237

8. P. Mogyorósi, T. Szörényi, K. Bali, Zs. Tóth, I. Hevesi: Appl. Surf. Sci.**36**, 157 (1989)

9. Zs. Tóth, Z. Kántor, P. Mogyorósi,T. Szörényi: In *Laser Assisted Processing II*, Proc. SPIE 1279, Ed. by L. D. Laude (1990) p. 150

10 I. W. Boyd: Laser Processing of Thin Films and Microstructures Springer Series in Materials Science 3 (Springer, Berlin - Heidelberg - New York - London - Paris - Tokyo) 1987.

11. C. O. Carlson, E. Stone, H. L. Bernstein, W. K. Tomita, W. C. Myers: Science,**154**, 1550 (1966)

12. V. J. Zaleckas, H. C. Koo: Appl. Phys. Lett. **31**, 615 (1977)

13. J. E. Andrew, P. E. Dyer, R. D. Greenough, P. H. Key: Appl. Phys. Lett **43**(11), 1076 (1983)

14. V. P. Veiko, S. M. Metev, A. I. Kaidanov, M. N. Libenson, E. B. Jakovlev: J. Phys. D: Appl. Phys. **13**, 1565 (1980)

15. R. J. Baseman, J. C. Andreshak, *Fundamentals of Beam-Solid Interactions and Transient Thermal Processing*, Proc. MRS 100, Ed. by M. J. Aziz, L E. Rehn, B. Stritzker (MRS, Pittsburgh 1988) p. 627

16. R. J. Baseman, N. M. Froberg, J. C. Andreshak, Z. Schlesinger:

Appl. Phys. Lett. **56**, 1412 (1990)

17. R. J. Baseman, N. M. Froberg, Appl. Phys. Lett. **55**, 1841 (1989)
18. J. S. Bakos, P. N. Ignácz, J. Szigeti, J. Kovács: Appl. Phys. Lett. **51**, 734 (1987)
19. R. M. Gilgenbach, P. L. Ventzek: Appl. Phys. Lett. **58**(15), 1597 (1991)
20. V. P. Veiko, A. I. Kaidanov: Vsesoiuznaia konferencija po vzaimodejstvo izlutsenie s veshestvom, 1990 Repino-Leningrad.
21. A. K. Jain, V. N. Kulkarni, D. K. Sood: Appl. Phys. **25**, 127 (1981)
22. R. C. Weast (ed.) *CRC Handbook of Chemistry and Physics 59th ed.* (CRC, Florida 1978-79)
23. Y. S. Touloukian (ed.) *Thermophysical Properties of Matter,* Volume 10, Thermal Diffusivity (IFI/Plenum, New York 1973)
24. L. E. Drain: The Laser Doppler Technique (A. Wiley - Interscience) 1980
25. ACS Symp. Ser. **351** (1987)
26. M. Leskelä, J. K. Truman, C. H. Mueller, P. H. Holloway: J. Vac.Sci. Technol. A **7**(6), 3147 (1989)
27. R. K. Williams, R. S. Graves, D. M. Kroeger, G. C. Marsh, J. O. Scarbrough, J. Brynestad: J. Appl. Phys. **66**(12), 6181 (1989)
28. S. B. Peralta, Z. H. Chen, A. Mindelis: Appl. Phys. A**52**, 289 (1991)
29. I. Terasaki, Y.Nakayama, K. Uchinokura, A. Maeda, T. Hasegawa, S. Tanaka: Jpn. J. Appl. Phys. **27**, L1480 (1988)
30. T. Hatou, Y. Takai, H. Hayakawa: Jpn. J. Appl. Phys. **27**, L617 (1988)
31. L. Baufay, D. Dispa, A. Pigeolet, L. D. Laude: J. Cryst. Growth **59**, 143 (1982)
32. R. Andrew, L. Baufay, A. Pigeolet, L. D. Laude: J. Appl. Phys. **53**, 4862 (1982)
33. L. Baufay, A. Pigeolet, L. D. Laude: J. Appl. Phys. **54**, 660 (1983)
34. C. Antoniadis, M. C. Joliet: Thin Solid Films, **115**, 75 (1984)
35. M. C. Joliet, C. Antoniadis, R. Andrew, L. D. Laude: Appl. Phys. Lett. **46**, 266 (1985)
36. L. D. Laude: Progr. Cryst. Growth Charact. **10**, 141 (1985)

37. L. D. Laude, M. Wautelet, R. Andrew: Appl. Phys. A **40**, 133 (1986)

38. Y. Canivez, A. Jadin, R. Andrew, L. D. Laude, M. Wautelet: In *Laser Processing and Diagnostics (II)*, eds.:D. Bauerle, K. L. Kompa, L. D. Laude, (Les Editions de Physique, Les Ulis 1986) p. 153

39. T. Szörényi, Z. Tóth: In *Laser Assisted Processing*, (Proc. SPIE 1022 Eds.: L. D. Laude, G. Rauscher, 1989) p. 93

40. Z. Tóth, T. Szörényi: Appl. Phys. A **52**, 273 (1991)

41. P. Tronc, M. Bensoussan, A. Brenac: Phys. Rev. B **8**, 5947 (1973)

42. H. Oheda: Japanese J. of Appl. Phys. **18**, 1973 (1979)

43. Z. Kántor, Z. Tóth, T. Szörényi: Appl. Phys. A **53** (1991) (in press)

44. Z. Tóth, T. Szörényi: Appl. Phys. Lett. to be published

Acknowledgements

First of all I thank the supports and encouragements of Dr. Tamás Szörényi my scientific supervisor who called my attention to this prosperous topic and introduced me into the every-day-life of research. I am indebted to Professor Zsolt Bor, Head of the Research Group on Laserphysics of the Hungarian Academy of Sciences and Professor Imre Hevesi, Head of the Department of Experimental Physics at József Attila University Szeged for their support and attention concerning my work. Special thanks are due to Professor Dieter Bäuerle, Head of Institute of Applied Physics of the Johannes Kepler University Linz for offering a fellowship in his institute and his encouragement to investigate the LIFT of high T_c superconducting ceramics. I am grateful to my colleagues; Dr. Péter Mogyorósi, Zoltán Kántor and Dr. Klaus Piglmayer for their assistance and invaluable discussions. Finally I wish to record my great thanks to László Horváth for his critical reading of the manusript and his valuable advice and to Edit Renkecz for the excellent figures.